Expression and Characterization of Ferredoxin and Flavin Adenine Dinucleotide Binding Domains of the Reductase Component of Soluble Methane Monooxygenase from *Methylococcus capsulatus* (Bath)†

Jessica L. Blazyk and Stephen J. Lippard*

Department of Chemistry, Massachusetts Institute of Technology, Cambridge, Massachusetts 02139

Received August 29, 2002; Revised Manuscript Received October 23, 2002

ABSTRACT: Soluble methane monooxygenase (sMMO) from *Methylococcus capsulatus* (Bath) catalyzes the selective oxidation of methane to methanol, the first step in the primary catabolic pathway of methanotrophic bacteria. A reductase (MMOR) mediates electron transfer from NADH through its FAD and [2Fe-2S] cofactors to the dinuclear non-heme iron sites housed in a hydroxylase (MMOH). The structurally distinct [2Fe-2S], FAD, and NADH binding domains of MMOR facilitated division of the protein into its functional ferredoxin (MMOR-Fd) and FAD/NADH (MMOR-FAD) component domains. The 10.9 kDa MMOR-Fd (MMOR residues 1−98) and 27.6 kDa MMOR-FAD (MMOR residues 99−348) were expressed and purified from recombinant *Escherichia coli* systems. The Fd and FAD domains have absorbance spectral features identical to those of the [2Fe-2S] and flavin components, respectively, of MMOR. Redox potentials, determined by reductive titrations that included indicator dyes, for the [2Fe-2S] and FAD cofactors in the domains are as follows: -205.2 ± 1.3 mV for $[2Fe\text{-}2S]_{ox/red}$, -172.4 ± 2.0 mV for $FAD_{ox/sq}$, and -266.4 ± 3.5 mV for $FAD_{sq/hq}$. Kinetic and spectral properties of intermediates observed in the reaction of oxidized MMOR-FAD (FAD_{ox}) with NADH at 4 °C were established with stopped-flow UV−visible spectroscopy. Analysis of the influence of pH on MMOR-FAD optical spectra, redox potentials, and NADH reaction kinetics afforded pK_a values for the semiquinone (FAD_{sq}) and hydroquinone (FAD_{hq}) MMOR-FAD species and two protonatable groups near the flavin cofactor. Electron transfer from MMOR-FAD_{hq} to oxidized MMOR-Fd is extremely slow ($k = 1500$ M^{-1} s^{-1} at 25 °C, compared to 90 s^{-1} at 4 °C for internal electron transfer between cofactors in MMOR), indicating that cofactor proximity is essential for efficient interdomain electron transfer.

Methanotrophic bacteria serve an important role in the carbon cycle by consuming methane produced in anaerobic sediments and thereby limiting the flux of this greenhouse gas into the atmosphere (*1*). The first step of the process, which is catalyzed by the enzyme methane monooxygenase (MMO),[1] involves the conversion of methane to methanol (eq 1). All methanotrophs express a membrane-bound

$$CH_4 + NADH + H^+ + O_2 \rightarrow CH_3OH + NAD^+ + H_2O \quad (1)$$

particulate MMO (pMMO), which contains copper (*2*). In the few species of methanotrophic bacteria capable of producing a second, soluble form of MMO (sMMO), differential expression of the two enzyme systems is regulated by the availability of copper ions. When the copper-to-biomass ratio is low, sMMO activity is observed, whereas pMMO is expressed at high copper-to-biomass ratios (*3*).

The sMMO complex from *Methylococcus capsulatus* (Bath) has been characterized extensively by a wide range of reactivity, spectroscopic, crystallographic, and kinetic methods (*4*−*9*). It comprises three proteins, a hydroxylase (MMOH, 251 kDa), a reductase (MMOR, 38.5 kDa), and a regulatory protein (MMOB, 15.9 kDa), all of which are required for catalytic function (*10*, *11*). Recent work demonstrates that a fourth protein, MMOD, is also involved in the sMMO system (*12*). The hydroxylase, a dimer of three subunits (*4*) in an $\alpha_2\beta_2\gamma_2$ configuration, contains two dinuclear carboxylate-bridged iron centers where dioxygen activation and methane hydroxylation occur. MMOR is an iron−sulfur flavoprotein that shuttles electrons from NADH to the hydroxylase to prime the enzyme system for reaction with dioxygen (*13*, *14*). The MMOR [2Fe-2S] center is located in the N-terminal portion of the protein and is significantly homologous with ferredoxins of plants, cyanobacteria, and archaebacteria (*15*). The C-terminal domain binds a single flavin adenine dinucleotide (FAD) molecule, which accepts two electrons from NADH. Electrons are then delivered one at a time to the [2Fe-2S] center for transfer to the hydroxylase diiron site (*11*, *14*, *16*).

MMOR belongs to a class of modular flavoprotein electron transferases (Figure 1), also called the ferredoxin:$NADP^+$ oxidoreductase (FNR) family. These proteins contain a flavin domain capable of accepting two electrons from a nicotinamide dinucleotide and a one-electron carrier domain, which may be linked or dissociable (*17*−*19*). The ability to attach the electron carrier domain to either the N- or C-terminal

† This work was supported by National Institutes of Health Research Grant GM32134 (S.J.L.). J.L.B. was a Howard Hughes Medical Institute predoctoral fellow.

* To whom correspondence should be addressed. E-mail: lippard@lippard.mit.edu. Telephone: (617) 253-1892. Fax: (617) 258-8150.

10.1021/bi026757f CCC: $22.00
Published on Web 12/05/2002

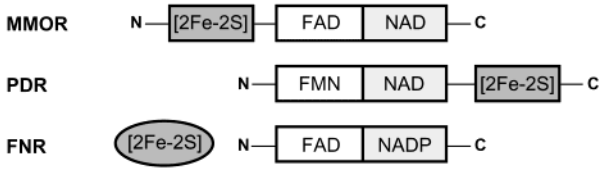

FIGURE 1: Examples of alternative connectivities between the one-electron carrier and flavin/NAD(P) binding domains of flavoprotein electron transferases.

end of the core flavin/NAD(P) protein implies that this domain is an independent modular unit. In accord with this notion, the crystal structure of *Burkholderia cepacia* phthalate dioxygenase reductase (PDR), a member of the FNR family, reveals distinct flavin mononucleotide (FMN), NADH binding, and [2Fe-2S] domains (*19*). Removal of the PDR [2Fe-2S] domain by fortuitous proteolytic cleavage produces a stable, truncated form amenable to biochemical characterization (*20*).

The highly modular nature of FNR family proteins suggested that dividing MMOR into its component ferredoxin (MMOR-Fd) and flavin/pyridine nucleotide (MMOR-FAD) domains should be feasible. The separate domain proteins were predicted to serve as useful models for studying the intra- and intermolecular electron transfer reactions of MMOR. In this paper, we report recombinant *Escherichia coli* systems for the high-yield expression of the individual MMOR domains. For both MMOR-Fd and MMOR-FAD, spectroscopic properties and redox potentials are examined and compared to those of MMOR. The kinetics of MMOR-FAD reduction with NADH and interdomain electron transfer reactions are described. An examination of the influence of pH on MMOR-FAD optical spectra, redox potentials, and NADH reaction kinetics is also presented. Ultimately, characterization of the individual electron transfer steps in the sMMO system, combined with the structures of MMOR and MMOH, will provide the means for tracing the electron transfer pathway from NADH through the flavin and [2Fe-2S] cofactors of MMOR into the carboxylate-bridged diiron active sites of MMOH.

[1] Abbreviations: MMO, methane monooxygenase; NAD^+ and NADH, oxidized and reduced forms, respectively, of nicotinamide adenine dinucleotide; pMMO, particulate methane monooxygenase; sMMO, soluble methane monooxygenase; MMOH, hydroxylase component of sMMO; MMOR, reductase component of sMMO; MMOB, coupling protein of sMMO; MMOD, fourth protein component of sMMO; FAD, flavin adenine dinucleotide; FNR, ferredoxin:$NADP^+$ oxidoreductase; PDR, phthalate dioxygenase reductase; MMOR-Fd, ferredoxin domain of MMOR (residues 1−98); MMOR-FAD, FAD/NADH domain of MMOR (residues 99−348); PCR, polymerase chain reaction; AP, alkaline phosphatase; EGTA, ethylene glycol bis(β-aminoethyl ether)-*N*,*N*,*N*′,*N*′-tetraacetic acid; LB, Luria-Bertani medium; Ap, ampicillin; IPTG, isopropyl thio-β-D-galactoside; MOPS, 3-(*N*-morpholino)propanesulfonic acid; DTT, 1,4-dithiothreitol; MMOR-Fd_{ox} (or Fd_{ox}) and MMOR-Fd_{red} (or Fd_{red}), oxidized and reduced forms of MMOR-Fd, respectively; MMOR-FAD_{ox} (or FAD_{ox}), MMOR-FAD_{sq} (or FAD_{sq}), and MMOR-FAD_{hq} (or FAD_{hq}), oxidized, semiquinone, and hydroquinone forms of MMOR-FAD, respectively; $MMOR_{3e-}$, fully reduced MMOR; MMOR-$FAD_{sq,max}$ and $MMOR_{sq,max}$, MMOR-FAD and MMOR, respectively, reduced such that the fraction of FAD_{sq} is maximized; EFA, evolving factor analysis; TAPS, *N*-[tris(hydroxymethyl)methyl]-3-aminopropanesulfonic acid; AQ2S, anthraquinone 2-sulfonate; AQ2,6S, anthraquinone 2,6-disulfonate; AQ1,5S, anthraquinone 1,5-disulfonate; $FAD_{ox/sq}$, midpoint potential of the FAD_{ox}/FAD_{sq} redox couple; $FAD_{sq/hq}$, midpoint potential of the FAD_{sq}/FAD_{hq} redox couple; $[2Fe\text{-}2S]_{ox/red}$, midpoint potential of the $[2Fe\text{-}2S]^{2+}$/$[2Fe\text{-}2S]^+$ redox couple; E_h, solution potential; MES, 2-(*N*-morpholino)-ethanesulfonic acid; FMN, flavin mononucleotide; CT1 and CT2, charge transfer intermediates 1 and 2, respectively, for the reaction of MMOR-FAD_{ox} and NADH.

MATERIALS AND METHODS

General Methods. The ferrozine method (*21*, *22*) was used to determine the iron content of MMOR-Fd; FAD determinations were performed as described in ref *16*. UV−visible spectra were obtained with an HP 8453 diode array spectrophotometer. Fluorescence excitation and emission scans were recorded with a Hitachi F-3010 fluorescence spectrophotometer.

MMOR Domain Selection. To define the Fd and FAD/NADH domain boundaries of *M. capsulatus* (Bath) MMOR, sections of MMOR were aligned with the full-length *B. cepacia* PDR protein sequence (PDB entry 2PIA) by using CLUSTAL W (*23*). In addition, the approximate MMOR domain sequences (residues 1−114, Fd domain; and residues 89−348, FAD/NADH domain) were compared to and aligned with other protein sequences in the nonredundant National Center for Biotechnology Information protein databases with the PSI-BLAST program. The C-terminal end of the MMOR-Fd domain was selected as residue 98, and the MMOR-FAD domain was designed to start at residue 99 after an obligatory methionine residue.

MMOR Domain Cloning. The Fd portion of the *mmoC* gene, which encodes MMOR (*15*), was amplified with *Pfu* DNA polymerase (Stratagene, La Jolla, CA) from pCH4 (*24*), obtained from J. C. Murrell (University of Warwick, Warwick, U.K.), by using the following primers: 5′-CG-**GAATTC**AACATTAAGGAGGTAAATTTATGCAG-CGAG-3′ and 5′-CCTCTCCA**AAGCTT**ATGCGTCAAT-GGGTATAG-3′. The primers 5′-CGAAGACCGACCTG-**GAATTC**TAAGGAGGTTATAATATGTGCCGCATCA-GTTTTGGTGAG-3′ and 5′-TCACAGTACTT**AAGCTT**T-TCAGGCCGCCCCGGAC-3′ were used to amplify the region of *mmoC* corresponding to the MMOR-FAD domain. The resulting 344 (Fd) and 809 bp (FAD) fragments were flanked by *Eco*RI and *Hin*dIII sites (boldface), which were introduced by the forward and reverse primers, respectively. The amplified DNA was purified from the PCRs by using the QIAquick PCR purification kit (Qiagen Inc., Valencia, CA). Both PCR products were digested with the restriction enzymes *Eco*RI and *Hin*dIII (New England Biolabs, Beverly, MA) by following the provided instructions. The high-copy number plasmid pKK223-3 (Amersham Pharmacia Biotech, Piscataway, NJ) was digested with the same restriction enzymes, and then treated with alkaline phosphatase (AP, Boehringer Mannheim, Indianapolis, IN) to prevent recircularization in the subsequent ligation reaction. After inactivating the AP by adding 20 mM EGTA and heating at 65 °C for 10 min, we isolated the DNA with the QIAquick PCR purification kit. The AP-treated pKK223-3 digest and *mmoC*-Fd or *mmoC*-FAD digest were ligated with T4 DNA ligase (New England Biolabs); the resulting plasmid solutions were transformed into *E. coli* XL1-Blue cells and plated on LB−ampicillin (Ap, 100 μg/mL) agar plates. Colonies with ampicillin resistance were analyzed further by restriction mapping of DNA obtained from plasmid minipreps. DNA sequencing [Massachusetts Institute of Technology (MIT) Biopolymers Laboratory] of positive pRED-Fd and pRED-FAD clones confirmed that the inserted genes contained no errors.

Expression and Purification of MMOR-Fd. The pRED-Fd(2) expression plasmid was transformed into *E. coli* JM105 cells. Cells were grown to saturation in 100 mL of LB−Ap (100 μg/mL) medium at 37 °C with 200 rpm shaking. To each of six 1 L quantities of LB−Ap (100 μg/mL) medium were added 10 mL of freshly prepared filter-sterilized 10 mM $Fe(NH_4)_2(SO_4)_2 \cdot 6H_2O$ in 100 mM sodium citrate (pH 7.0) and 10 mL of the saturated JM105/pRED-Fd(2) starter culture. When the OD_{660} reached 0.6, the cultures were supplemented with 80 μM Fe^{2+}, added as 2 mL of a 40 mM $FeSO_4 \cdot 7H_2O$ solution in 12.5 mM H_2SO_4 per liter of cell culture, and induction was started by adding IPTG to a final concentration of 1.0 mM. After 3.5 h, the cells were collected by centrifugation and then suspended in 100 mL of cold cracking buffer [25 mM MOPS (pH 7.0), 1 mM DTT, 5 mM $MgCl_2$, and 200 μM $Fe(NH_4)_2(SO_4)_2 \cdot 6H_2O$] containing DNase (1.5 units/mL) and 1 mM Pefabloc SC. The cells were sonicated on ice with three 2 min pulses at 40% output (Branson Sonifier model 450 equipped with a $^3/_4$ in. horn) and then centrifuged for 40 min at 98000*g* to separate the soluble and insoluble material. The soluble cell extract was filtered through a 0.2 μm membrane and loaded onto a DEAE-Sepharose CL-6B (Amersham Pharmacia) column (2.6 cm × 15 cm) equilibrated with buffer A [25 mM MOPS (pH 7.0), 1 mM DTT, and 50 mM NaCl]. After a 120 mL wash with buffer A, proteins were eluted with a 740 mL linear gradient from buffer A to buffer B [25 mM MOPS (pH 7.0), 1 mM DTT, and 500 mM NaCl]. MMOR-Fd eluted at approximately 370 mM NaCl. Fractions containing MMOR-Fd were identified by optical spectroscopy and SDS−PAGE and then pooled and concentrated by ultrafiltration. This crude Fd protein solution was filtered through a 0.2 μm membrane and applied to a Superdex 75 (Amersham Pharmacia) size-exclusion column (2.6 cm × 60 cm) equilibrated with 25 mM MOPS (pH 7.0) containing 1 mM DTT and 150 mM NaCl. Fractions were pooled on the basis of color and SDS−PAGE analysis. Typical preparations yielded 12−14 mg of >98% pure MMOR-Fd (98 residues, MW = 10 931) per liter of *E. coli* expression culture.

Expression and Purification of MMOR-FAD. A 100 mL JM105/pRED-FAD(1) culture in LB−Ap (100 μg/mL) medium was grown to saturation at 37 °C with shaking at 200 rpm. Each of six 1 L quantities of LB−Ap (100 μg/mL) medium was inoculated with 10 mL of the saturated starter culture and transferred to a 37 °C incubator set to rotate at 200 rpm. When the OD_{660} reached ca. 0.6, expression of the MMOR-FAD domain was induced with 1.0 mM IPTG. After 3.5 h, the cells were collected by centrifugation, suspended in 100 mL of cracking buffer, and sonicated as described above. The soluble cell extract was obtained by centrifugation for 40 min at 98000*g* followed by filtration through a 0.2 μm membrane. The first chromatographic step, resolution on a DEAE-Sepharose CL-6B anion exchange column, was performed exactly as described for MMOR-Fd. Fractions containing the FAD domain, which eluted at approximately 240 mM NaCl, were identified by SDS−PAGE and pooled. Half of this crude material was loaded onto a 5′-AMP Sepharose (Sigma, St. Louis, MO) column (2.6 cm × 18 cm) equilibrated with buffer A. The column was washed with 25 mM MOPS (pH 7.0), 1 mM DTT containing 95 mM NaCl (70 mL), 410 mM NaCl (50 mL), and then 50 mM NaCl (175 mL) to remove protein contaminants. The FAD domain was eluted with buffer B containing 1 mM NADH. All of the fractions collected in the NADH wash were combined as pure MMOR-FAD domain and concentrated over a YM10 Amicon membrane. The FAD domain was exchanged into 25 mM MOPS (pH 7.0) and 2 mM DTT with a Biogel P6 desalting column (Bio-Rad, Hercules, CA). This procedure typically afforded 25 mg of >95% pure MMOR-FAD (250 residues, MW = 27 629) per liter of expression culture.

Expression and Purification of MMOR. Full-length MMOR was prepared from a recombinant *E. coli* expression system exactly as described previously (*16*), except that iron was added to the medium as described for MMOR-Fd domain expression.

Mass Spectrometric Analysis. Pure MMOR-Fd and MMOR-FAD proteins in 25 mM MOPS (pH 7.0) were submitted to the MIT Biopolymers Laboratory for analysis by electrospray ionization mass spectrometry (ESI-MS). To remove cofactors which separated from the proteins upon treatment with ammonium acetate, formic acid, and acetonitrile, HPLC purification was necessary. The protein component was analyzed with a Sciex model API 365 triple-stage mass spectrometer.

EPR Spectroscopy. MMOR-Fd and MMOR in 25 mM potassium phosphate buffer (pH 7.0) were made anaerobic by vacuum gas exchange with O_2-free N_2. In an anaerobic chamber, protein, anaerobic buffer, and sodium dithionite were combined to yield 258 μM protein solutions containing a 2-fold molar excess of dithionite (i.e., 500 μM for MMOR-Fd and 1.5 mM for MMOR). After equilibration for several minutes, aliquots of the reduced protein samples were transferred to EPR tubes and frozen in liquid nitrogen.

With estimates of the MMOR (and MMOR-FAD) midpoint potentials of −174, −206 (MMOR only), and −265 mV (vide infra), the maximum amount of semiquinone species that can be stabilized was calculated. Plots of species concentration (FAD_{ox}, FAD_{sq}, and FAD_{hq} for MMOR-FAD, also Fd_{ox} and Fd_{red} for MMOR) versus solution potential were constructed with KaleidaGraph, version 3.0 or 3.51 (Synergy Software, Reading, PA). Wavelengths (590 nm for MMOR-FAD and 640 nm for MMOR) for monitoring the titrations were selected such that the maximum absorbance and maximum fraction of semiquinone species (0.75) coincided. A 900 μL quantity of MMOR-FAD [159 μM in 25 mM potassium phosphate (pH 7.0)] was made anaerobic in a sealed quartz cuvette by vacuum gas exchange and titrated with sodium dithionite (ca. 4 mM) to maximize the FAD_{sq} species; this objective was achieved by reducing the sample until A_{590} was maximal. In a similar fashion, the MMOR protein [900 μL of 170 μM protein in 25 mM potassium phosphate (pH 7.0)] was reduced to the point of maximum FAD_{sq} species by maximizing A_{640}. After dithionite additions, the MMOR-FAD and MMOR concentrations were calculated as 148 and 153 μM, respectively, of which ∼75% of the FAD cofactor (ca. 110 μM) was expected to be in the semiquinone oxidation state. In an anaerobic chamber, aliquots of the semiquinone samples were transferred to EPR tubes.

EPR spectra of the four samples ($MMOR\text{-}Fd_{red}$, $MMOR_{3e-}$, $MMOR\text{-}FAD_{sq,max}$, and $MMOR_{sq,max}$) were recorded with a Bruker EMX spectrometer fitted with an Oxford ESR 900 liquid helium cryostat. The temperature was maintained at

10 K for the first two samples (reduced [2Fe-2S]) and 100 K for the latter two samples (FAD_{sq}). The power saturation behavior of each protein sample was examined, and a high-quality spectrum was collected at a power at which the signal was not saturated.

Determination of the FAD_{sq} Optical Spectrum by EFA. To examine the optical spectra of MMOR-FAD in various oxidation states, anaerobic reductive titrations were performed. A 1.00 mL aliquot of 90 μM MMOR-FAD in 25 mM potassium phosphate (pH 7.0) was transferred to a sealed quartz cuvette and made anaerobic with 10−12 cycles of vacuum gas exchange with O_2-free N_2. Aliquots of 1−2 mM sodium dithionite were added with a gastight Hamilton titrating syringe. After each addition, optical spectra were collected until no further changes were observed (usually less than 5 min), and the final spectrum was saved for data analysis. The temperature for the titration experiments was held constant at 25 °C with a circulating water bath.

After subtracting the average absorbance between 800 and 900 nm from each spectrum, we applied dilution corrections. The evolving factor analysis (EFA) function resident in the Specfit Global Analysis software suite (version 2.10U or 3.0.16, Spectrum Software Associates, Chapel Hill, NC) was used to extract component spectra for the MMOR-FAD domain, corresponding to the oxidized (FAD_{ox}), semiquinone (FAD_{sq}), and hydroquinone (FAD_{hq}) forms of the protein. Noniterative EFA was performed for each data set to generate extinction coefficient profiles for the three spectroscopically distinct MMOR-FAD oxidation states. The extinction coefficients were scaled such that $\epsilon_{458} = 11\,000\ M^{-1}\ cm^{-1}$ for FAD_{ox}. To test the validity of this method, the individual spectra collected during the reductive titrations were fit with linear combinations of the oxidized, semiquinone, and hydroquinone component spectra (KaleidaGraph).

pH Effects on the Optical Spectra of MMOR Domains. To investigate the effects of pH on the optical spectra of the MMOR-Fd and MMOR-FAD proteins, samples of the oxidized and reduced domains were examined at varying pH values. Fourteen buffers were prepared for these experiments: 100 mM sodium citrate (pH 4.92, 5.06, 5.21, 5.47, and 5.81), 100 mM potassium phosphate (pH 6.00, 6.49, 6.98, 7.50, and 8.02), and 100 mM TAPS (pH 8.07, 8.50, 8.98, and 9.10). MMOR-FAD_{ox} (214 μM) in 1 mM potassium phosphate (pH 7.0) was combined with each of these buffers to yield ~40 μM protein solutions. Each solution was allowed to equilibrate for ~2 min, and an optical spectrum (300−900 nm) was recorded. The temperature was maintained at 25 °C with a circulating water bath. To determine the pK_a for the observed optical change, plots of A_{450} or A_{500} versus pH were fit with the expressions shown in eqs 2 and 3, respectively, by using the program KaleidaGraph. To yield ~45 μM MMOR-Fd_{ox} solutions, MMOR-Fd in 1 mM potassium phosphate (pH 7.0) was mixed with 100 mM sodium citrate (pH 5.47), 100 mM potassium phosphate (pH 6.00, 6.98, or 8.02), or 100 mM TAPS (pH 8.98). After a brief equilibration, optical spectra (300−900 nm) were collected at room temperature.

$$A = A_{max} - \frac{A_{max} - A_{min}}{1 + 10^{pH - pK_a}} \quad (2)$$

$$A = A_{min} - \frac{A_{max} - A_{min}}{1 + 10^{pH - pK_a}} \quad (3)$$

Fd_{red} and FAD_{hq} samples were prepared at varying pH values by reducing the proteins with sodium dithionite in an anaerobic chamber, dialyzing away excess dithionite, and combining aliquots of the reduced proteins with strong buffers (same as those used for the Fd_{ox} experiment described above). Sealed MMOR-Fd_{red} and MMOR-FAD_{hq} samples were removed from the box, and optical spectra (300−900 nm) were recorded. For all samples, the temperature was held constant at 25 °C with a circulating water bath.

To examine the effects of pH on the optical spectrum of MMOR-FAD_{sq}, anaerobic reductive titrations of MMOR-FAD were performed at varying pHs. The following buffers were used in these experiments: 80 mM potassium phosphate (pH 6.00), 60 mM potassium phosphate (pH 6.49), 75 mM potassium phosphate (pH 6.98), 70 mM potassium phosphate (pH 8.02), and 75 mM TAPS (pH 8.50, 8.98, or 9.31). The MMOR-FAD domain (ca. 50 μM) in a total volume of 1.00 mL was reduced with dithionite exactly as described above. After each addition of reductant, equilibrium was usually achieved in 5−10 min, but took as long as 40 min at high pH values. Data were processed as described, and EFA afforded FAD_{ox}, FAD_{sq}, and FAD_{hq} component spectra for each titration data set.

Redox Potential Determinations for the MMOR Domains. The equilibrium midpoint potentials of the MMOR-Fd and MMOR-FAD domains were determined by using a series of reductive titrations. All of the titrations were performed in 25 mM potassium phosphate (pH 7.0) buffer because MOPS, the standard buffer used in sMMO studies, interferes with electron equilibration. Each titration included one or more redox active indicator dyes with known midpoint potentials to permit calculation of the solution potential throughout the titration. Dyes used for MMOR-Fd potential determination included anthraquinone 2-sulfonate (AQ2S; $E^{\circ\prime} = -226$ mV), phenosafranine ($E^{\circ\prime} = -252$ mV), and anthraquinone 2,6-disulfonate (AQ2,6S; $E^{\circ\prime} = -184$ mV) in combination with phenosafranine (15−20% relative to AQ2,6S).

The MMOR-Fd domain (ca. 40 μM) and dye(s) (ca. 35 μM for AQ2S and AQ2,6S and ca. 12 μM for phenosafranine) in a total volume of 1.00 mL were placed in a sealed quartz cuvette and made anaerobic with 12 cycles of vacuum gas exchange with O_2-free N_2. A gastight Hamilton titrating syringe was filled with a solution of sodium dithionite (1−2 mM) in phosphate buffer and then transferred to the cuvette under positive pressure. After the solution had equilibrated to 25 °C, an initial visible spectrum (300−900 nm) of the oxidized material was collected. Dithionite was added to the protein/dye solution in 5 μL aliquots; the solution was mixed thoroughly, and a spectrum was recorded. Multiple scans were taken after each dithionite addition until the system had reached equilibrium (usually 5−10 min, but as long as 40 min). The final spectrum was saved for data analysis. This process was repeated until the protein and dye(s) were reduced completely. In addition, the MMOR-Fd potential was measured in the presence of MMOH (0.5 equiv) and/or MMOB (1 equiv) with AQ2S as the solution potential indicator.

The equilibrium midpoint potentials of the MMOR-FAD domain were determined by using the same method. The

indicator dyes AQ2S, anthraquinone 1,5-disulfonate (AQ1,5S; $E^{\circ\prime} = -172$ mV), phenosafranine, safranine O ($E^{\circ\prime} = -289$ mV), and AQ2,6S in combination with phenosafranine (15−20% relative to AQ2,6S) were used for the MMOR-FAD domain reductive titrations. The MMOR-FAD protein (ca. 30 μM) and dye(s) (ca. 35 μM for AQ2S, AQ1,5S, and AQ2,6S and ca. 12 μM for phenosafranine and safranine O) were titrated at 25 °C with sodium dithionite.

To obtain dye component spectra, an anaerobic solution of each dye (1.00 mL, 65−70 μM for the anthraquinone dyes and 20 μM for phenosafranine and safranine O) was titrated with 1−2 mM sodium dithionite. The initial spectrum was taken as the oxidized dye component spectrum. After baseline and dilution corrections had been performed, the first spectrum for which no optical changes were observed upon dithionite addition was selected as the fully reduced dye spectrum. The MMOR-Fd component spectra, Fd_{ox} and Fd_{red}, were also determined by titration with dithionite; the MMOR-FAD component spectra, FAD_{ox}, FAD_{sq}, and FAD_{hq}, were obtained by EFA as described above. For each redox couple (dye_{ox}/dye_{red}, Fd_{ox}/Fd_{red}, FAD_{ox}/FAD_{sq}, and FAD_{sq}/FAD_{hq}), a difference spectrum, $\Delta\epsilon_i(\lambda)$, was calculated by subtracting the extinction coefficients of the oxidized species from those of the reduced species.

Dilution corrections were applied to each spectrum in a titration data set. To eliminate any errors due to inaccurate extinction coefficients, the initial species concentrations were determined by fitting the initial oxidized spectrum with a linear combination of oxidized protein and oxidized indicator spectra (KaleidaGraph). A difference spectrum for each titration point was generated by subtracting the starting oxidized spectrum from each spectrum in the data set. These difference spectra (350 nm $\leq \lambda \leq$ 800 nm) were then fit with linear combinations of component difference spectra, as shown in eq 4. The concentration differences, Δc_i, returned

$$\Delta A(\lambda) = \sum \Delta\epsilon_i(\lambda)(\Delta c_i) \tag{4}$$

by fitting with eq 4 were readily converted to species concentrations by comparison with the total concentrations of protein and dye(s). The solution potential and MMOR domain midpoint potentials were computed for each titration point with modified Nernst equations (*16*). Average MMOR-Fd and MMOR-FAD midpoint potentials were calculated by including only those data for which the solution potential was within 40 mV of both the approximate MMOR-Fd or MMOR-FAD domain potential and the indicator potential.

Relative redox potentials were determined for the FAD domain at varying pH values. For each MMOR-FAD reductive titration (vide supra), a species fraction (FAD_{ox}, FAD_{sq}, or FAD_{hq}) versus percent reduction plot was constructed, where the latter was computed according to eq 5.

$$\%\ \text{reduction} = 100\left(\frac{0.5[FAD_{sq}] + [FAD_{hq}]}{[FAD]_T}\right) \tag{5}$$

The FAD_{sq} versus percent reduction plots were fit manually by generating a series of curves representing different ΔE° values (difference between the $FAD_{ox/sq}$ and $FAD_{sq/hq}$ redox potentials). First, given various ΔE° values, theoretical fractions of FAD_{ox}, FAD_{sq}, and FAD_{hq} were calculated over a range of solution potentials ($E_h = -500$ to 100 mV) with eqs 6−8, respectively.

$$X_{ox} = \frac{[FAD_{ox}]}{[FAD]_T} = \frac{\exp\left[-\frac{F}{RT}(FAD_{ox/sq} - E_h)\right]}{\exp\left[-\frac{F}{RT}(FAD_{ox/sq} - E_h)\right] + 1 + \exp\left[\frac{F}{RT}(FAD_{sq/hq} - E_h)\right]} \tag{6}$$

$$X_{sq} = \frac{[FAD_{sq}]}{[FAD]_T} = \frac{1}{\exp\left[-\frac{F}{RT}(FAD_{ox/sq} - E_h)\right] + 1 + \exp\left[\frac{F}{RT}(FAD_{sq/hq} - E_h)\right]} \tag{7}$$

$$X_{hq} = \frac{[FAD_{hq}]}{[FAD]_T} = \frac{\exp\left[\frac{F}{RT}(FAD_{sq/hq} - E_h)\right]}{\exp\left[-\frac{F}{RT}(FAD_{ox/sq} - E_h)\right] + 1 + \exp\left[\frac{F}{RT}(FAD_{sq/hq} - E_h)\right]} \tag{8}$$

For each E_h value, the percent reduction (eq 5) was calculated. Finally, the theoretical mole fraction versus % reduction curves were compared to the experimental data in KaleidaGraph; the ΔE° value used to generate the best-fitting curve was taken as the difference in redox potentials at that pH.

Isothermal Titration Calorimetry. A VP-ITC isothermal titration calorimeter (MicroCal, Inc., Northampton, MA) was used to measure the binding affinity of the FAD_{ox}−NAD^+ complex. All titrations were performed at 4.2 °C in 25 mM MOPS (pH 7.0). Titrant (1.89 mM NAD^+) was injected in 10 μL aliquots from a 250 μL stirred titration syringe into the 1.430 mL sample cell containing 43 μM MMOR-FAD. Stirring was maintained at 310 rpm throughout the titrations. To measure the heat of dilution for NAD^+, the experiment was repeated with buffer in the sample cell. Data were integrated and fit with the MicroCal Origin version 5.0 software package.

MMOR-FAD Reaction with NADH. To examine intramolecular electron transfer for the reduction of MMOR-FAD with NADH, several stopped-flow experiments were performed. A Hi-Tech Scientific SF-61 DX2 double-mixing stopped-flow spectrophotometer configured for either single-wavelength photomultiplier or multiwavelength diode array collection was used for all experiments. Prior to use, the stopped-flow apparatus was made anaerobic by flushing the syringes and flow cell with a solution of ca. 5 mM sodium dithionite. The dithionite was then flushed from the system with anaerobic buffer. Oxidized MMOR-FAD protein in 25 mM MOPS (pH 7.0) was made anaerobic with 12−15 cycles of vacuum gas exchange with O_2-free N_2. Anaerobic NADH solutions were prepared by bubbling with nitrogen for at least 15 min. Concentrations of MMOR-FAD were 20−40 μM after mixing; NADH concentrations were ~10 times that of MMOR-FAD, except where noted. The MMOR-FAD reaction with NADH was monitored at 458, 625, and 725 nm in

Table 1: Properties of MMOR-Fd, MMOR-FAD, and MMOR

	MMOR-Fd	MMOR-FAD	MMOR
MW measured (Da)	10929.0[a] ± 1.1	27629.0[b] ± 2.4	38546.9 ± 3.9[c]
ϵ_{458} (M^{-1} cm^{-1}) at pH 7.0 and 25 °C	9550 ± 200	11000 ± 500	20800 ± 1000[d]
λ_{max} (nm) at pH 7.0 and 25 °C	332, 418, 467	394, 458	332, 394, 458[c]
g values (fully reduced)[e]	2.049, 1.958, 1.888	n/a	2.047, 1.958, 1.871
g values (maximum FAD_{sq})	n/a	2.004[f]	2.005[g]
$FAD_{ox/sq}$ (mV) at pH 7.0 and 25 °C	n/a	−172.4 ± 2.0	−176 ± 7[c]
$[2Fe\text{-}2S]_{ox/red}$ (mV) at pH 7.0 and 25 °C	−205.2 ± 1.3	n/a	−209 ± 14[c]
$FAD_{sq/hq}$ (mV) at pH 7.0 and 25 °C	n/a	−266.4 ± 3.5	−266 ± 15[c]

[a] Expected value of 10 931.3 Da for the apoprotein with the N-terminal methionine intact. [b] Expected value of 27 628.3 Da for the apoprotein with the N-terminal methionine cleaved. [c] As reported in ref *16*. [d] As reported in ref *11*. [e] EPR recorded at 10 K and 500 μW at 9.478 GHz, with a modulation amplitude of 10.0 G. [f] EPR recorded at 100 K and 32 μW at 9.478 GHz with a modulation amplitude of 2.0 G. [g] EPR recorded at 100 K and 127 μW at 9.482 GHz, with a modulation amplitude of 2.0 G.

single-wavelength photomultiplier mode. Data points (512) were collected in 1 s shots on a log time scale. The experiment was repeated with the stopped-flow apparatus in multiwavelength diode array mode. For each 1.4 or 2 s shot, 160 spectra (295−705 or 370−740 nm) were recorded with a logarithmic time base. The temperature was maintained at 4 °C with a constant-temperature circulating water bath for all experiments. Single-wavelength absorbance data were fit to a sum of two or three exponential decays with the program KinetAsyst 2, version 2.2 (Hi-Tech Limited, Salisbury, England). The Specfit program was used to analyze diode array data and second-order reaction data.

MMOR-FAD reduction with NADH was also investigated over a range of pH values. For these experiments, the FAD domain was prepared in 1 mM MOPS (pH 7.0) and 49 mM NaCl and mixed with strongly buffered NADH solutions at the desired pH. Buffers included were 50 mM MES (pH 5.47, 5.93, and 6.29), 50 mM MOPS (pH 6.70, 7.00, and 7.40), and 50 mM TAPS (pH 7.77, 8.21, and 8.47). The ionic strength was maintained at 50 mM by addition of appropriate quantities of NaCl to each buffer. pK_a values for pH-dependent effects were calculated by using eqs 2 and 3.

Interdomain Electron Transfer Reactions. Electron transfer reactions between (a) $MMOR\text{-}FAD_{hq}$ and $MMOR\text{-}Fd_{ox}$, (b) $MMOR\text{-}FAD_{hq}$ and $MMOR\text{-}FAD_{ox}$, and (c) $MMOR\text{-}Fd_{ox}$/$MMOR\text{-}FAD_{ox}$ and NADH were investigated by stopped-flow optical spectroscopy. All experiments were performed in 25 mM MOPS (pH 7.0) or 25 mM potassium phosphate (pH 7.0) at 4 and/or 25 °C. Single-wavelength photomultiplier data collection was used for reactions b and c; the multiwavelength diode array mode was employed for reactions a and b. Protein concentrations after mixing were 20−30 μM, except where noted.

RESULTS

General Characterization of MMOR Domains. Both MMOR-Fd (MMOR residues 1−98) and MMOR-FAD (MMOR residues 99−348) were prepared in good yield from recombinant expression systems. Protein purity and cofactor content were monitored effectively by examining absorbance ratios. For MMOR-Fd, an A_{276}/A_{332} ratio of 1.05 indicates pure, fully complemented protein; pure MMOR-FAD has an A_{270}/A_{458} ratio of ~6.7. Molecular weights within experimental error of the calculated values for the apoproteins (N-terminal methionine intact for the Fd domain and cleaved for the FAD domain) were obtained by mass spectrometric analysis (Table 1). Iron and FAD determinations were used to calculate extinction coefficients for the domains, assuming 2.0 mol of Fe/mol of MMOR-Fd and 1.0 mol of FAD/mol of MMOR-FAD. The EPR spectra of fully reduced MMOR-Fd and full-length MMOR exhibit rhombic signals characteristic of mixed-valent $[2Fe\text{-}2S]^+$ centers with nearly identical *g* values. Although the EPR spectra of $FAD_{sq,max}$ and $MMOR_{sq,max}$ are essentially identical, the power saturation behavior for these samples is somewhat different, presumably due to the presence of EPR-active $[2Fe\text{-}2S]^+$ (ca. 60% of total [2Fe-2S]) in the $MMOR_{sq,max}$ sample. The UV−visible spectra for the MMOR domains can be added to yield a spectrum identical to that of full-length MMOR (Figure 2). Full-length MMOR is not very fluorescent, which was previously believed to be due to quenching of the FAD fluorescence by the nearby [2Fe-2S] center. Fluorescence studies of MMOR-FAD and free FMN demonstrated that the FAD domain is also a weak fluorophore; therefore, the protein environment around the FAD cofactor must quench most of the flavin fluorescence.

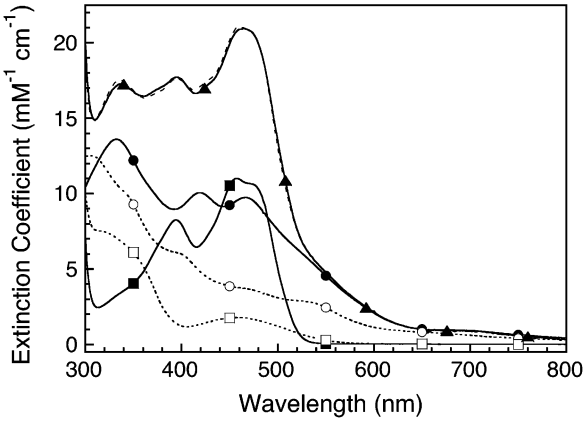

FIGURE 2: Optical spectra at pH 7.0 of MMOR-Fd (circles) and MMOR-FAD (squares) in the fully oxidized (filled symbols and solid lines) and fully reduced (empty symbols and dotted lines) oxidation states. The sum of the two oxidized domain spectra (dashed line) is superimposed on the MMOR optical spectrum (triangles).

Evolving Factor Analysis for MMOR-FAD Component Spectra. Selected spectra from a reductive titration of MMOR-FAD at pH 7.0 are shown in Figure 3A. The FAD_{ox}, FAD_{sq}, and FAD_{hq} component spectra extracted by evolving factor analysis are displayed in Figure 3B. The generated component spectra fit the original titration data extremely well; in addition, the total calculated concentration of MMOR-FAD (the sum of the FAD_{ox}, FAD_{sq}, and FAD_{hq} concentrations) is constant for all of the titration spectra,

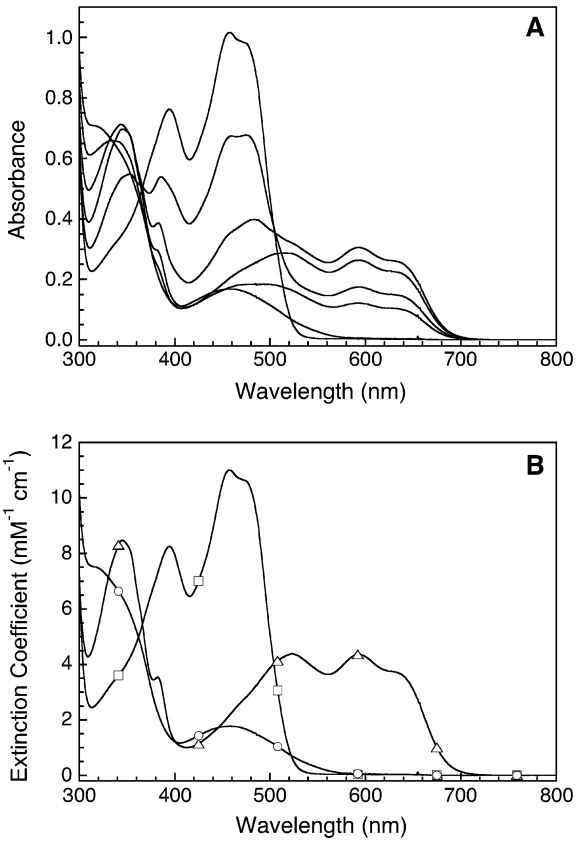

FIGURE 3: Determination of the FAD_{sq} optical spectrum at pH 7.0. (A) Selected spectra from an anaerobic reductive titration of 91 μM MMOR-FAD with ~2 mM dithionite at 25 °C. (B) Component spectra, which correspond to the FAD_{ox} (□), FAD_{sq} (△), and FAD_{hq} (○) oxidation states, derived from evolving factor analysis of the titration data.

showing that the component spectra are correctly scaled with respect to each other.

Effect of pH on the Optical Spectra of MMOR Domains. Below pH 5.5, the Fd and FAD domains precipitate from solution, so the effective range for the pH investigations was 5.5−9.3. Over this pH range, the oxidized and reduced MMOR-Fd spectra did not exhibit pH-dependent optical changes. The UV−visible spectra of all three MMOR-FAD chromophores (FAD_{ox}, FAD_{sq}, and FAD_{hq}) are altered by pH (Figure 4A). Data corresponding to the wavelengths at which maximum absorbance changes occur reflect processes having pK_a values of 6.55 ± 0.05 (Figure 4B) and 7.1 ± 0.2 (Figure 4C) for FAD_{ox} and FAD_{hq}, respectively. Above pH 8.5, the FAD_{sq} spectra provide evidence for deprotonation of the blue neutral semiquinone species to form a red anionic semiquinone (*25*). There were not enough data to determine an accurate pK_a for this transition, but the value must be at least 9.

Redox Potentials of MMOR-Fd and MMOR-FAD. Figure 5 shows selected difference spectra from a reductive titration of MMOR-FAD in the presence of the indicator phenosafranine. To examine the accuracy of difference fitting, global fits to both difference spectra and the original titration spectra were performed for a reductive titration of MMOR-Fd and AQ2S. The returned $[2Fe\text{-}2S]_{ox/red}$ $E^{\circ\prime}$ values (−205.1 ± 1.3 mV for difference fitting and −208.3 ± 3.8 mV for direct fitting) are essentially identical, except that direct fitting results in a larger standard deviation. Difference spectra

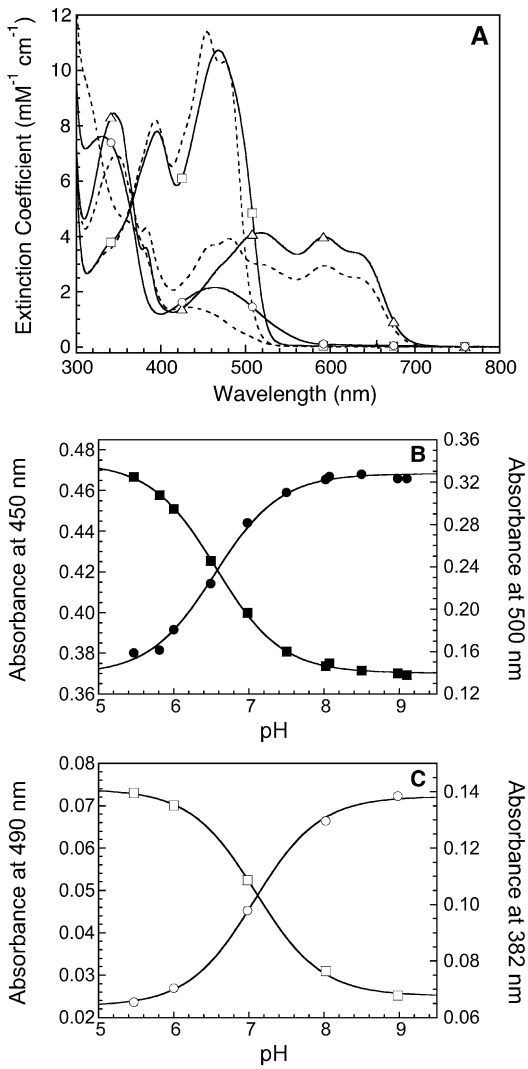

FIGURE 4: Effect of pH on the MMOR-FAD optical spectra. (A) FAD_{ox} (□), FAD_{sq} (△), and FAD_{hq} (○) component spectra determined at pH 6 (—) and 9 (- - -). (B) FAD_{ox} absorbance at 450 (●) and 500 nm (■) as a function of pH. (C) Variation of FAD_{hq} absorbance at 382 (○) and 490 nm (□) with pH. Solid lines in panels B and C are fits to eqs 2 and 3.

emphasize the changes in a sample so that even small spectral differences can be fit accurately when not obscured by much larger (and unchanged) features. In addition, difference fitting in many cases reduces the number of independent variables in a fit so that a unique solution may be calculated. Therefore, fitting difference spectra is the method used to calculate component concentrations for all of the redox potential determinations.

Plots of MMOR domain potential versus solution potential were constructed to aid in selecting the data range included in the overall midpoint potential averages. Only those titration points that returned a relatively constant potential over a range of solution potentials were selected. In general, this linear range correlates well with the arbitrary selection of data points with solution potentials within 40 mV of both the estimated domain potential and indicator potential. It was necessary to correct the safranine O range from the calculated values of −250 to −304 mV to a range of −266 to −322 mV. The calculated midpoint potentials for MMOR-Fd ($[2Fe\text{-}2S]_{ox/red}$) and MMOR-FAD ($FAD_{ox/sq}$ and $FAD_{sq/hq}$) are displayed in Table 1. Within experimental error, addition of

Scheme 1

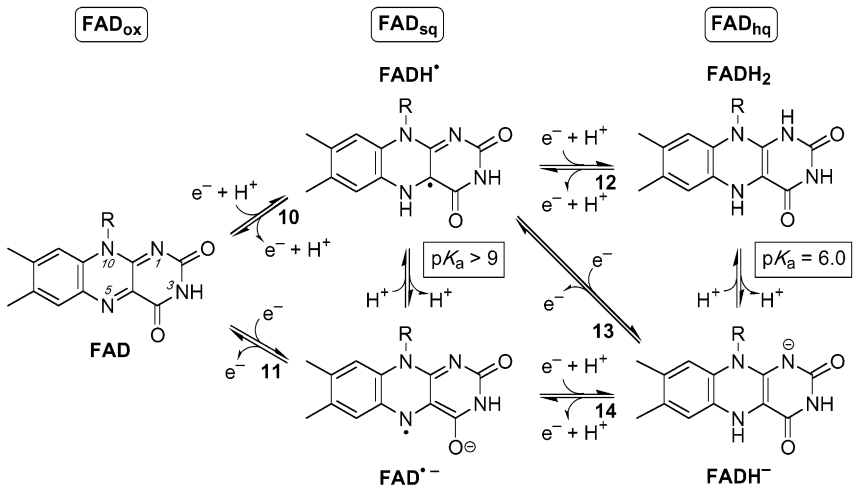

0.5 equiv of MMOH and/or 1 equiv of MMOB to MMOR-Fd does not alter the Fd domain potential. MMOH forms complexes with both MMOB (*11*) and MMOR-Fd (*26*); by analogy to MMOR (*11*, *16*, *27*), MMOR-Fd is not expected to bind MMOB.

Relative MMOR-FAD redox potentials were determined by analyzing reductive titrations of the FAD domain performed at varying pH values. Because no indicator dye was included in these titrations, the solution potential at each titration point is unknown, and only the difference between the $FAD_{ox/sq}$ and $FAD_{sq/hq}$ potentials may be computed. Fits to mole fraction versus % reduction plots generated $\Delta E°$ ($FAD_{ox/sq} - FAD_{sq/hq}$) values for each titration, as shown in Figure 6A. The MMOR-FAD $\Delta E°$ values increase from 80 mV at pH 6.0, the lowest pH that was examined, to a maximum of 94 mV at pH 7.0, and then decrease to 32 mV at pH 9.0, the highest pH that was examined (Figure 6B). Additional titrations to extend the pH range could not be performed due to protein precipitation at low pH and extremely slow equilibration at high pH.

To analyze these data further, it was necessary to account for protons involved in the redox equilibria. For a reductive reaction that includes a single proton, the measured midpoint potential varies linearly with pH, as shown in eq 9.

$$E_m = E°' + \frac{RT}{nF}\ln[H^+] = E°' - \left(\frac{2.303RT}{nF}\right)pH \quad (9)$$

Therefore, the redox potential for a one-electron ($n = 1$), one-proton process exhibits a pH dependence of −59 mV/pH unit at 25 °C. Scheme 1 depicts the relevant redox equilibria for MMOR-FAD. At pH values below the FAD_{sq} pK_a (>9), reduction of FAD_{ox} to the neutral semiquinone state requires a proton (eq 10); above this pK_a value, formation of anionic semiquinone is proton-independent (eq 11).

$$FAD + e^- + H^+ \rightarrow FADH^{\bullet} \quad (10)$$

$$FAD + e^- \rightarrow FAD^{\bullet -} \quad (11)$$

Thus, the $FAD_{ox/sq}$ redox potential should vary by −59 mV/pH unit at low pH and not at all at high pH [Figure 6C (···)]. For semiquinone reduction to hydroquinone, there are three possible redox equilibria (eqs 12−14).

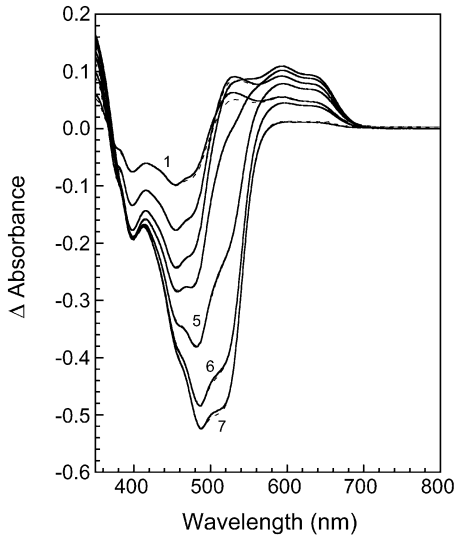

FIGURE 5: Difference spectra for the reductive titration of a 1 mL mixture of 30 μM MMOR-FAD and 11 μM phenosafranine by dithionite at pH 7.0 and 25 °C. Spectra 1−7 correspond to the addition of 20, 30, 40, 50, 70, 90, and 110 μL of ~2 mM dithionite, respectively. Fits (- - -) are superimposed on the difference spectra.

$$FADH^{\bullet} + e^- + H^+ \rightarrow FADH_2 \quad (12)$$

$$FADH^{\bullet} + e^- \rightarrow FADH^- \quad (13)$$

$$FAD^{\bullet -} + e^- + H^+ \rightarrow FADH^- \quad (14)$$

At low and high pH values (eqs 12 and 14, respectively), the redox reactions include protons. Between the FAD_{hq} and FAD_{sq} pK_a values (6.0 and >9, respectively, vide infra), reduction proceeds without protonation (eq 13). Therefore, the $FAD_{sq/hq}$ potential should be constant between pH 6 and ~9 and vary by −59 mV/pH unit at low and high pH [Figure 6C (- - -)]. Combining these processes yields a ΔE value ($FAD_{ox/sq} - FAD_{sq/hq}$) that is constant below pH 6, decreases by 59 mV/pH unit between pH 6 and ~9, and increases by 59 mV/pH unit above pH ~9 [Figure 6C (—)].

To identify pH-dependent changes in MMOR-FAD redox potentials due to the protein environment, the contributions to $\Delta E°$ by the redox equilibria were subtracted from the $\Delta E°$ versus pH data. An appropriate ΔE correction curve was constructed with slopes of 0, −59, and 59 mV/pH unit at

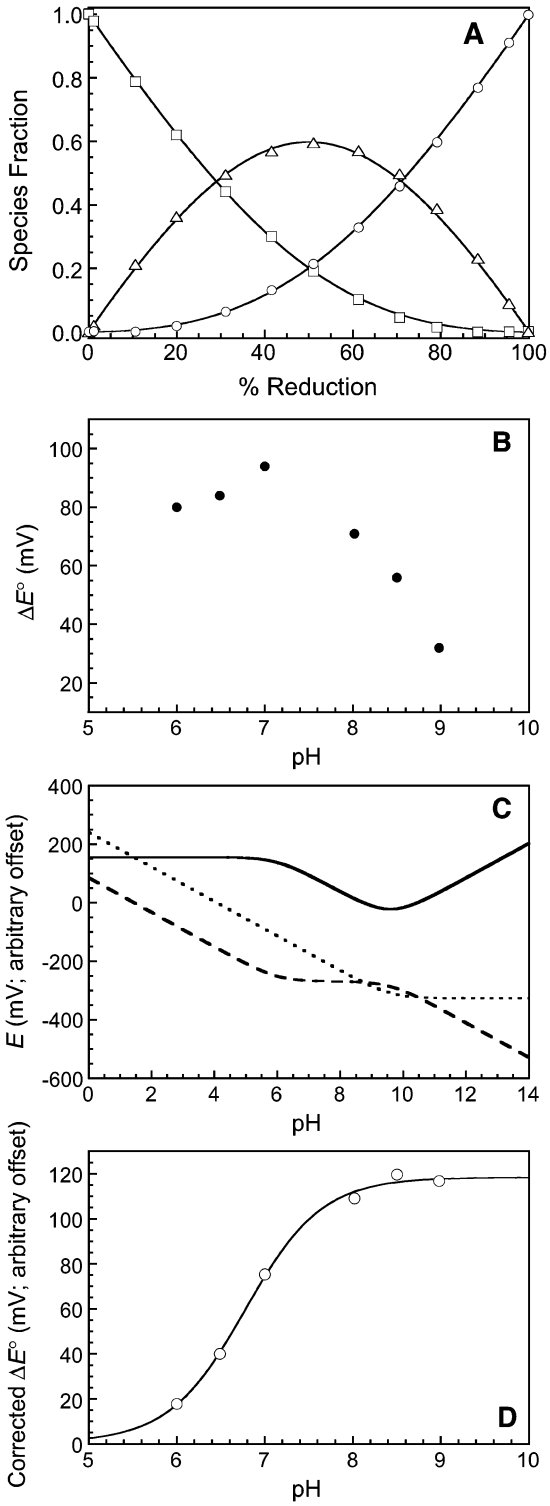

FIGURE 6: pH dependence of the relative redox potentials of MMOR-FAD. (A) MMOR-FAD reductive titration data obtained at pH 8.5 with fits (—) determined by using eqs 5−8: FAD_{ox} (□), FAD_{sq} (△), and FAD_{hq} (○). (B) Variation of the difference between the two MMOR-FAD redox potentials with pH. (C) Theoretical curves reflecting the pH dependence of $FAD_{ox/sq}$ (···), $FAD_{sq/hq}$ (- - -), and ΔE [$FAD_{ox/sq}$ − $FAD_{sq/hq}$ (—)] due to the inclusion of protons in some of the redox equilibria (Scheme 1). FAD_{hq} and FAD_{sq} pK_a values of 6.0 and 9.6, respectively, are shown. (D) pH dependence of $\Delta E°$ values after subtraction of redox equilibria-related effects (C). The solid line represents a fit to eq 3.

low, middle, and high pH, respectively, with transitions corresponding to pK_a values of 6.0 and ≥9 (Figure 6C).

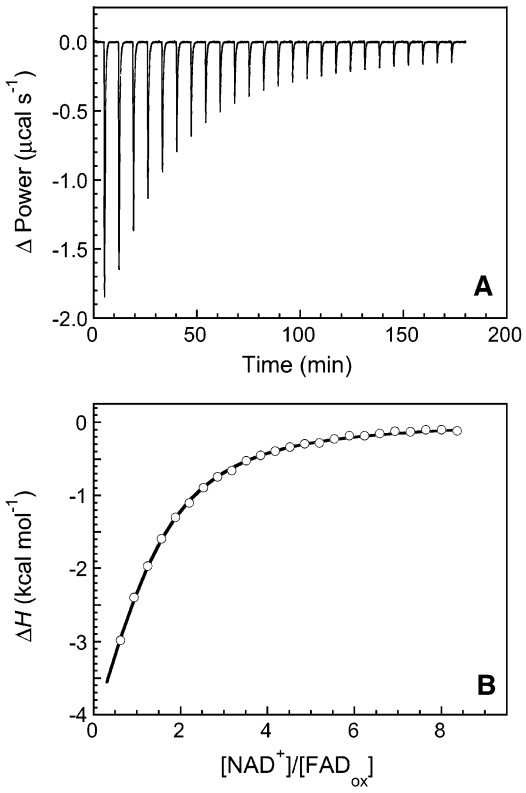

FIGURE 7: Determination of the MMOR-FAD_{ox}−NAD^+ binding constant by isothermal titration calorimetry. (A) Data recorded for the formation of the complex between FAD_{ox} (43 μM in the calorimeter cell) and NAD^+ (1.89 mM in a 250 μL injection syringe) at 4.2 °C. Each heat pulse corresponds to a 10 μL injection into the 1.430 mL sample cell. (B) Integrated enthalpy data (○) fit with a one-site binding model (—).

Because the precise FAD_{sq} pK_a value is unknown, this procedure was repeated for 13 pK_a values between 9.0 and 11.4. Subtracting the ΔE correction curves from the MMOR-FAD $\Delta E°$ versus pH data yielded titration curves that reflect a process with a pK_a of 6.8 ± 0.1 and a redox potential change of 119 ± 4 mV (Figure 6D).

Measurement of the MMOR-FAD_{ox}−NAD^+ Binding Constant. The binding affinity of NAD^+ for MMOR-FAD_{ox} was determined by isothermal titration calorimetry. Figure 7A shows the power required to compensate for the exothermic binding reaction after each addition of titrant to the sample cell. By integrating these heat pulses with respect to time, we calculated the incremental heat change for each injection. A plot of these data as a function of the NAD^+/MMOR-FAD molar ratio is presented in Figure 7B. Fitting with the one-site model resident in the Origin software yielded the following thermodynamic parameters for the FAD_{ox}−NAD^+ binding reaction: $K_d = 43 \pm 2$ μM, $N = 1.00 \pm 0.05$ binding sites per FAD_{ox} molecule; $\Delta G = -5.5$ kcal/mol; $\Delta H = -7.7 \pm 0.4$ kcal/mol; and $T\Delta S = -2.2$ kcal/mol [Figure 7B (—)].

Kinetics of MMOR-FAD Reduction with NADH. Reduction of the MMOR-FAD domain with NADH was studied by diode array stopped-flow UV−visible spectroscopy. A typical data set collected for this reaction at pH 7.0 and 4 °C is shown in Figure 8A. Spectra corresponding to four intermediates were resolved with Specfit software by using a sequential four-component model with a fixed FAD_{ox} spectrum as the initial species (Figure 8B). When NADH binds to the MMOR-FAD domain, species CT1, which is

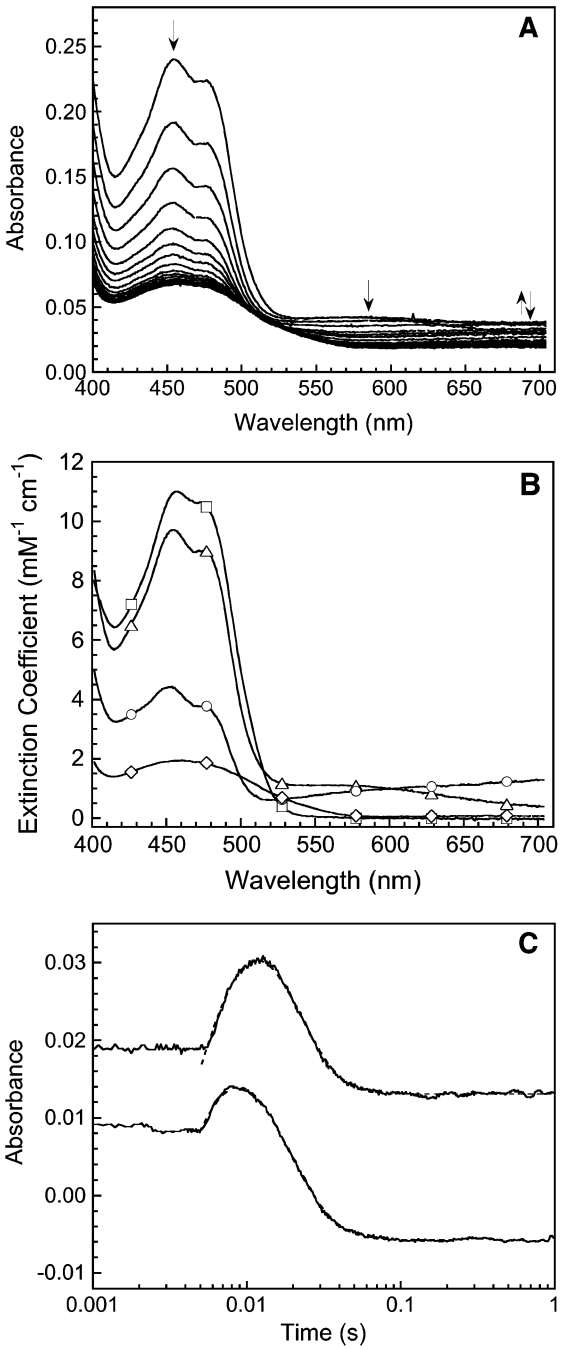

FIGURE 8: Kinetics of MMOR-FAD reduction with NADH. (A) Spectra recorded at ~3 ms intervals by diode array stopped-flow spectroscopy in the first 67 ms after mixing 25 μM FAD_{ox} with 250 μM NADH at 4 °C and pH 7.0. (B) Spectra of intermediates resolved by global analysis of the diode array kinetic data: FAD_{ox} (□), CT1 (△), CT2 (○), and FAD_{hq} (◇). (C) Time-dependent absorbance changes at 625 (bottom trace) and 725 nm for this reaction. For clarity, the 725 nm trace was offset by 0.02 absorbance unit. Dashed lines represent fits to the data.

characterized by a charge transfer interaction between the NADH nicotinamide ring and flavin isoalloxazine group ($\lambda_{max} \approx 570$ nm), is formed. Hydride transfer from NADH to the oxidized FAD produces intermediate CT2, which exhibits a lower-energy charge transfer band ($\lambda_{max} > 700$ nm) between the NAD^+ and reduced flavin (FAD_{hq}) groups. The CT2 species decays as NAD^+ is released from the fully reduced MMOR-FAD protein. The NADH reaction with the FAD domain is summarized in Scheme 2.

Single-wavelength stopped-flow data collected at 458, 625, and 725 nm were fit with sums of two or three exponential decays (Figure 8C). CT1 formation is observed as an increase in A_{625} at <7 ms; CT2 formation produces an increase in A_{725} at <10 ms. Decreases in both A_{625} and A_{725} at >10 ms correspond to CT2 decay to FAD_{hq}. All three transitions are reflected as decreases in A_{458}. Rate constants of 350 ± 20 (vide infra), 188 ± 7, and 89 ± 4 s^{-1} were determined for CT1 formation, CT1 decay/CT2 formation, and CT2 decay, respectively, at pH 7.0 and 4 °C.

To investigate NADH binding to MMOR-FAD, single-wavelength stopped-flow experiments were performed with varying concentrations of NADH. The rate of CT1 formation increases hyperbolically with NADH concentration (Figure 9), which indicates that a spectroscopically silent intermediate, denoted MC1 for Michaelis complex 1, must precede CT1, the first observed intermediate. By fitting these data with a hyperbolic expression, a K_d value of 25 ± 4 μM was calculated for the FAD domain−NADH binding interaction at 4 °C. Under saturating NADH conditions, the rate constant for CT1 formation, k_1, approaches 350 s^{-1}. In addition, at low NADH concentrations, the rate of CT2 formation converges with the slower CT1 formation rate (data not shown), further substantiating the kinetic model.

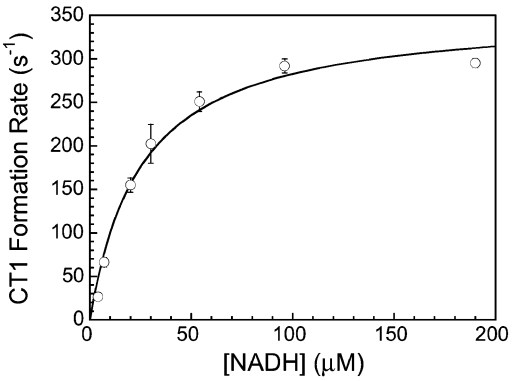

FIGURE 9: Dependence of the CT1 formation rate constant, k_1, on NADH concentration for the reduction of MMOR-FAD with NADH at 4 °C and pH 7.0. The solid line represents a hyperbolic fit to the data.

Effect of pH on the Reaction of MMOR-FAD with NADH. Reduction of MMOR-FAD with NADH was also investigated at nine pH values in the range of 5.5−8.5. Reaction rates were determined from single-wavelength stopped-flow data collected at each pH value; these results are displayed in Figure 10A. CT1 formation (k_1) and CT2 formation (k_2) are somewhat faster at low pH; in addition, k_1, and possibly k_2, may increase slightly at high pH. The variation of k_1 with respect to pH reflects either two processes having pK_a values of 6.61 ± 0.07 and 7.09 ± 0.08 [Figure 10A (—)] or a single process with a pK_a of 6.2 ± 0.1 (fit not shown). The minimum k_1 value, 230 s^{-1}, occurs near pH 7.0. At low and high pH, k_1 approaches 372 and 274 s^{-1}, respectively. The k_2 data can also be fit fairly well with these pK_a values. The rate of CT2 decay, k_3, is unchanged throughout this pH range.

Diode array stopped-flow experiments were performed for this reaction at five pH values between 5.5 and 8.5. Spectra corresponding to the FAD_{ox}, CT1, CT2, and FAD_{hq} intermediates were resolved with Specfit software by using a sequential four-component model with a fixed FAD_{ox}

Scheme 2

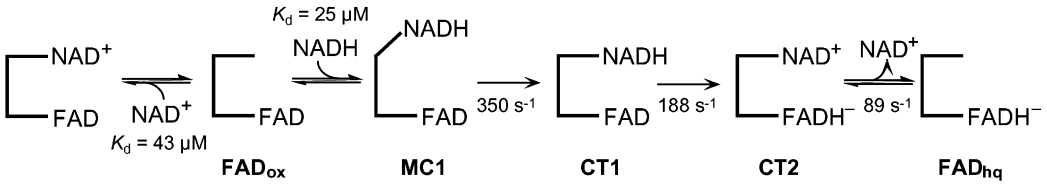

spectrum (initial species) determined at the appropriate pH. CT1 spectra are essentially unchanged over this pH range; FAD_{hq} spectra vary as determined above (Figure 4A,C). The CT2 intermediate spectrum, however, is significantly altered as a function of pH, as shown in Figure 10B. Large increases in CT2 absorbance between 400 and 500 nm accompany pH decreases. Reducing the pH also converts the CT2 charge transfer band from one characteristic of a FADH−NAD^+ complex ($\lambda_{max} > 700$ nm) to one very similar to the FAD−NADH charge transfer band ($\lambda_{max} \approx 570$ nm) of CT1. In fact, the CT1 and CT2 intermediates determined for data sets collected at pH 5.47 have nearly identical charge transfer bands; therefore, these data can be fit equally well with a sequential three-component model. The changes in CT2 ϵ_{470} and ϵ_{700} values with pH reflect a pK_a of 6.0 ± 0.1 (Figure 10C).

Interdomain Electron Transfer Reactions. Reduction of full-length MMOR with NADH proceeds in exactly the same manner described for MMOR-FAD, except that NAD^+ release (CT2 decay) is accompanied by electron transfer from the FAD_{hq} cofactor to the $[2Fe\text{-}2S]^{2+}$ cluster, yielding the FAD_{sq} and $[2Fe\text{-}2S]^+$ oxidation states (*11*, *14*, *16*, *28*). Therefore, electron transfer between the MMOR domains was investigated to determine the effects of separating the domains. Electron transfer from MMOR-FAD_{hq} to Fd_{ox} at 25 °C can be fit as a second-order reaction (A + B → C) with an observed rate constant k of 1500 ± 100 M^{-1} s^{-1} (Figure 11A). Within a reasonable range of Fd_{ox} concentrations (12.5−50 μM), the second-order rate constant for electron transfer from 12.5 μM MMOR-FAD_{hq} is unchanged. A pseudo-first-order rate constant could not be determined for this reaction due to the high concentration of MMOR-Fd, estimated to be greater than 0.2 M, required to saturate the MMOR-FAD binding site. To examine the possibility that interdomain electron transfer is slow because MMOR-FAD−MMOR-Fd binding is slow, the domains were pre-complexed and allowed to react with NADH in a stopped-flow experiment. Although the CT1 and CT2 formation and decay rate constants are unchanged, electron transfer to the Fd domain is still extremely slow, even at increased temperatures. For the comproportionation reaction of MMOR-FAD_{ox} and MMOR-FAD_{hq} to form MMOR-FAD_{sq} at 4 °C, there is a single observed step, which was fit with a second-order model (Figure 11B). The observed rate constant for electron transfer (k = 100 ± 15 M^{-1} s^{-1}) describes a slow reaction that should not interfere with the NADH reaction kinetics reported above for MMOR-FAD.

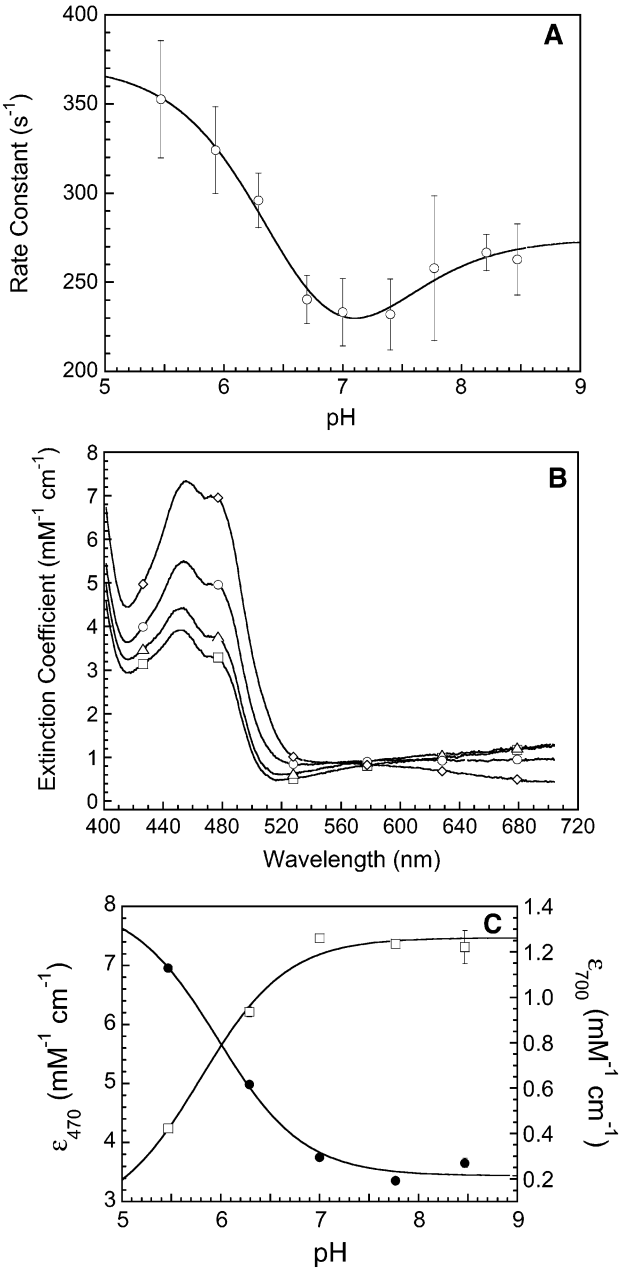

FIGURE 10: Influence of pH on the reaction of MMOR-FAD with NADH at 4 °C. (A) Variation of k_1 (CT1 formation) with pH. The solid line is a fit of the type defined in eqs 2 and 3. (B) CT2 spectra determined at pH 7.77 (□), 7.00 (△), 6.29 (○), and 5.47 (◇). (C) CT2 extinction coefficients at 470 (●) and 700 nm (□) with respect to pH. Solid lines are fits to eqs 2 and 3.

DISCUSSION

Recombinant MMOR Domains. High-yield recombinant expression systems were developed for both the ferredoxin and FAD/NADH domains of MMOR. The NMR solution structure of the MMOR-Fd domain shows that this protein adopts a compact three-dimensional fold similar to that of other plant-type ferredoxins (*29*). Preliminary NMR studies of the MMOR-FAD protein demonstrate that it too forms a well-defined structure in solution.[2] In nearly every respect

[2] J. Müller, G. Wagner, and S. J. Lippard, unpublished results.

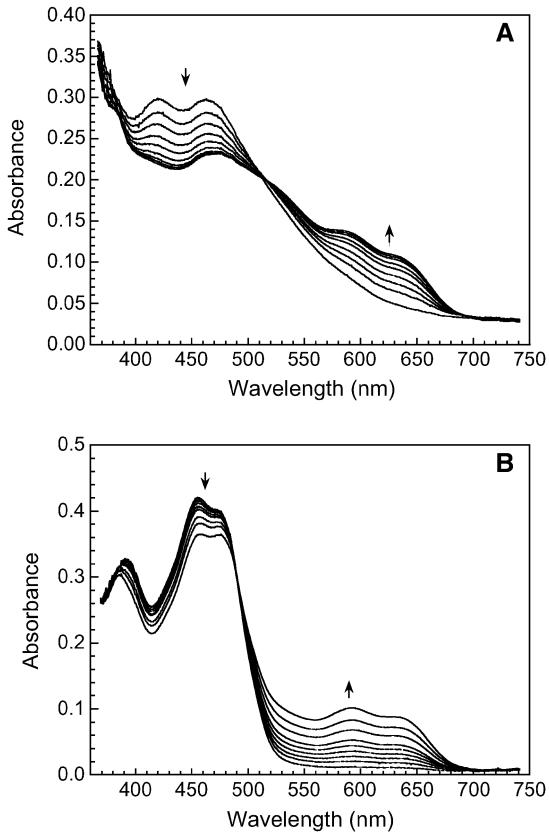

FIGURE 11: Electron transfer from MMOR-FAD_{hq} to Fd_{ox} or MMOR-FAD_{ox}. (A) Diode array spectra collected during the first 380 s after mixing 30 μM MMOR-FAD_{hq} and 30 μM Fd_{ox} at 25 °C and pH 7.0. (B) Diode array spectra collected during the first 380 s after mixing 30 μM MMOR-FAD_{hq} and 30 μM MMOR-FAD_{ox} at 4 °C and pH 7.0. Second-order rate constants were determined by fitting the data with second-order kinetic models in Specfit.

that has been examined, MMOR-Fd and MMOR-FAD are extremely good models for these domains in the full-length reductase. As judged by optical and EPR spectroscopy, the domain cofactors are in protein environments nearly identical to those of MMOR. By separation of the MMOR domains, the complexity of the full-length protein is reduced without compromising the integrity of most biochemical properties. For some experiments, the domains afford more straightforward data interpretation when compared to the corresponding MMOR study; for others, the MMOR domains provide data that could not have been obtained with the full-length reductase.

For example, the domains have been instrumental in structurally characterizing MMOR. The solution structure of the 10.9 kDa Fd domain was completed recently (*29*), a feat that would have been far more challenging for the 38.5 kDa MMOR. Determination of high-quality Fd_{ox}, Fd_{red}, FAD_{ox}, FAD_{sq}, and FAD_{hq} component spectra required separation of the [2Fe-2S] and flavin cofactors; these component spectra were essential for accurate determinations of the MMOR redox potentials (*16*). Furthermore, pH-associated optical changes observed for MMOR could not be assigned to individual chromophores without examining MMOR-Fd and MMOR-FAD separately.

Redox Potentials of MMOR-Fd and MMOR-FAD. The redox potentials measured for MMOR-Fd and MMOR-FAD match closely those reported previously for full-length MMOR (Table 1) (*13*, *16*). Therefore, it appears that the ferredoxin domain of MMOR exerts no effect on the FAD midpoint potentials (or vice versa). Because data fitting for the MMOR domains required fewer independent parameters (two or three) than that for MMOR (four or five), the domain potentials are more precise, as reflected by the significantly smaller standard deviations. The $FAD_{ox/sq}$ potential for MMOR-FAD (-172 ± 2 mV) agrees better with the value reported recently for MMOR [-176 ± 7 mV (*16*)] than with a previous determination [-150 ± 20 mV (*13*)], although all three potentials are within experimental error of each other. The method employed for the MMOR domain and recent MMOR (*16*) redox potential studies has several advantages, including the avoidance of dyes that bind to the investigated proteins, simultaneous data fitting over the entire visible region, the production of multiple potential measurements for each experiment, and collection of all data at a single regulated temperature. For these reasons, the lower $FAD_{ox/sq}$ midpoint potential determined with this method is probably more accurate.

Addition of MMOH or MMOB does not affect the MMOR-Fd midpoint potential within experimental error. A lag phase preceding Fd reduction was observed in titrations that included MMOH, presumably due to electron transfer to the MMOH diiron sites mediated by the Fd domain. As found for the full-length reductase (*26*), the lag phase appeared to be shorter when MMOB was also included in the titration. If it is assumed that there is no kinetic block to full electron equilibration, this result reflects a shift in the MMOH midpoint potential, a thermodynamic property. Therefore, the MMOH redox potential in the MMOH−MMOB−MMOR-Fd complex appears to be lower than that in the MMOH−MMOR-Fd complex, a difference that agrees with measurements of the *Methylosinus trichosporium* OB3b MMOH potentials in MMOH−MMOB−MMOR and MMOH−MMOR complexes (*30*).

Reaction of MMOR-FAD with NADH. The following kinetic model, which accounts for the results of stopped-flow optical experiments, is proposed for the reduction of the FAD domain with NADH at pH 7.0 and 4 °C (Scheme 2). The chemistry for this reaction corresponds directly with the first steps of the MMOR−NADH reaction (*11*, *16*). In the first step, NADH binds rapidly to MMOR-FAD, forming a Michaelis complex, MC1, with an optical spectrum identical to that of MMOR-FAD_{ox}. The K_d value for this interaction is 25 ± 4 μM (Figure 9). Isothermal titration calorimetry experiments yielded a K_d of 43 ± 2 μM for NAD^+ binding to FAD_{ox} (Figure 7). MMOR binds NADH significantly more tightly with a measured K_d value of 3.8 μM (*16*). This result suggests that the NADH binding site of MMOR-FAD differs from that of full-length MMOR. Possibilities for this reduced NADH−FAD_{ox} binding affinity include structural or hydrogen bonding perturbations near the NADH binding site.

A conformational change, which occurs with an observed rate constant of 350 s^{-1} at pH 7.0, gives rise to the FAD−NADH charge transfer interaction of intermediate CT1. Because of the relatively weak FAD_{ox}−NADH binding ($K_d = 25$ μM), a 30-fold excess of NADH is required to approach the 350 s^{-1} limit for CT1 formation. Since many experiments were performed with only a 10-fold excess of NADH, the observed rate constant for this step was typically 290 ± 20

s^{-1} (Figure 8). In the MMOR−NADH reaction, CT1 formation proceeds at the same rate ($k = 350\ s^{-1}$ at 4 °C) with saturating NADH (*16*).

Hydride transfer from NADH to FAD produces the CT2 intermediate with a rate constant of 188 s^{-1}. This species is characterized by a FADH−NAD^+ charge transfer band that is more intense and lower in energy than the FAD−NADH charge transfer band of CT1. Release of NAD^+, yielding the hydroquinone form of MMOR-FAD, occurs with a rate constant of 89 s^{-1}. The rate constants for the corresponding steps of the MMOR−NADH reaction, 190 and 90 s^{-1}, respectively, are nearly identical (*16*). It appears that, once NADH binds to MMOR-FAD, the electron transfer steps proceed exactly as reported for MMOR. In full-length MMOR, CT2 decay is accompanied by electron transfer from the reduced flavin cofactor to the [2Fe-2S] cluster, generating a species, SQ, comprising mainly FAD_{sq} and Fd_{red} (*11*, *16*). Electron transfer between the two MMOR cofactors occurs with a rate constant of 130 s^{-1}, as measured in a pH jump experiment (*16*). On the basis of this result, it was proposed that the slower electron transfer rate constant (90 s^{-1}) observed in the MMOR−NADH reaction is limited by the rate of NAD^+ release. The CT2 decay rate constant reported here for the isolated NAD^+ release step in MMOR-FAD (89 s^{-1}) supports this theory.

Influence of pH on MMOR-FAD Spectral, Redox, and Kinetic Properties. The UV−visible spectra of FAD_{ox}, FAD_{sq}, and FAD_{hq} species all exhibit pH-dependent changes, as depicted in Figure 4, with pK_a values of 6.55 ± 0.05, >9, and 7.1 ± 0.2, respectively. As observed by extinction coefficient increases around 300 nm and decreases above 500 nm at high pH, the FAD_{sq} optical transition represents deprotonation of the blue neutral semiquinone to form a red species characteristic of anionic flavin semiquinone (Scheme 1). The macroscopic pK_a values observed for the FAD_{ox} and FAD_{hq} chromophores are most likely associated with protonatable groups near or hydrogen bonded to the flavin isoalloxazine moiety rather than direct protonation of the flavin itself. Protonation of protein-bound flavins in the hydroquinone oxidation state typically occurs with a pK_a of <6 (*31*), so the pK_a of 7.1 noted for the FAD_{hq} optical spectrum probably corresponds to a different protonation event.

Equilibrium reductive titrations of MMOR-FAD at varying pH values show that $\Delta E°$ ($FAD_{ox/sq} - FAD_{sq/hq}$) is maximized near pH 7.0 (Figure 6B). Above or below this pH, the difference in potentials is diminished. Via correction for the flavin redox equilibria-linked ΔE contributions, a protein-dependent pK_a of 6.8 ± 0.1 for the MMOR-FAD $\Delta E°$ values is revealed (Figure 6D). This pK_a value may reflect the combined effects of the two protein-associated pK_a values (6.6 and 7.1) determined for the MMOR-FAD optical spectra and CT1 formation rate constant (vide infra). Because the measured $\Delta E°$ values reflect the difference between $FAD_{ox/sq}$ and $FAD_{sq/hq}$, either or both potentials may be affected by protonation of the protein environment. The corresponding MMOR $\Delta E°$ values exhibit a similar trend, with reported pK_a values of 6.6 ± 0.5 and 7.6 ± 0.9 (*16*). Analyzing the MMOR $\Delta E°$ versus pH data (Figure 8 in ref *16*) in the same manner described here for MMOR-FAD yields a single pK_a of 6.5 ± 0.2 for $\Delta E°$ variation.[3]

Kinetic studies of the MMOR-FAD reduction with NADH at varying pH values revealed several interesting pH-dependent features of this reaction. The CT1 formation rate constant, k_1 in Scheme 2, increases at low pH and possibly also at high pH. In addition, the CT1 decay/CT2 formation rate constant exhibits a similar, but less pronounced, variation with pH. The k_1 data could be fit as either one (pK_a = 6.2 ± 0.1) or two (pK_a = 6.61 ± 0.07 and 7.09 ± 0.08) pH-dependent processes (Figure 10A). Compared to the single-pK_a model, the two-pK_a model generates a better fit to the k_1 versus pH data and is therefore favored. Moreover, the pK_a values calculated for this fit exactly match those determined for pH-dependent changes in the FAD_{ox} (pK_a = 6.55 ± 0.05) and FAD_{hq} (pK_a = 7.1 ± 0.2) optical spectra. Formation of the CT1 intermediate is presumed to represent a conformational change that orients the pyridine nucleotide and flavin isoalloxazine groups for efficient electron transfer, as indicated by the appearance of a FAD−NADH charge transfer band. Such a conformational reorganization step could easily be influenced by protonatable amino acid side chains hydrogen bonded to or in the vicinity of the prosthetic groups. The nature of these processes may be clarified when the structure of MMOR-FAD is available. At pH <6, the k_1 value for the MMOR-FAD reaction with NADH reaches the value reported for this step (350 s^{-1}) in the corresponding MMOR reaction (*16*). The amino acid side chain responsible for the k_1 variation in MMOR-FAD may be protected from deprotonation or have an altered pK_a in MMOR. Alternatively, a more extensive hydrogen bonding network in MMOR, including contacts between the Fd and FAD domains, may make this residue less relevant for orienting the cofactors in MMOR. The weaker binding of NADH to MMOR-FAD (25 μM) compared to the binding of MMOR (3.8 μM) may also arise from a slightly perturbed hydrogen bonding network in the NADH binding cavity, possibly due to the same side chain that affects the CT1 formation rate constant. In fact, the variation in k_1 with pH may simply reflect differences in NADH binding affinity such that the NADH binding site is saturated only at low pH.

Spectra corresponding to the kinetic intermediates observed in the MMOR-FAD reaction with NADH were resolved by global analysis of diode array stopped-flow data. Over the pH range of 5.5−8.5, the CT1 spectrum is unchanged; the CT2 intermediate, however, undergoes significant optical changes that reflect a pK_a of 6.0 ± 0.1 (Figure 10B,C). At pH 5.5, the CT2 optical spectrum closely resembles the CT1 intermediate, particularly at λ > 530 nm. The charge transfer bands for these two species are essentially indistinguishable. This phenomenon arises from protonation at flavin position N1 of anionic FAD_{hq} ($FADH^-$) to form $FADH_2$ (Scheme 1). The charge transfer interaction between neutral $FADH_2$ and NAD^+ is significantly weaker than that between $FADH^-$ and NAD^+ but quite similar to the FAD−NADH charge transfer interaction of CT1. The measured FAD_{hq} pK_a for MMOR-FAD is within the range of values determined by NMR for N1 protonation in other flavoproteins (*31*). A similar pK_a of 6.2 ± 0.1 was attributed to protonation of the flavin N1 site in MMOR (*16*).

The pK_a values of ~6.5 and 6.8 noted for the FAD_{ox} optical spectrum and $\Delta E°$ values, respectively, may cor-

[3] J. L. Blazyk, D. A. Kopp, and S. J. Lippard, unpublished results.

respond to one or more carboxylate groups near the N1 and/or N3 position(s) of the flavin isoalloxazine ring system. Similar pK_a values have been attributed to carboxylate moieties near the flavin cofactors of other flavoproteins (*32*, *33*). Deprotonation of the carboxylate(s) would destabilize the anionic FAD_{hq}, thereby decreasing the $FAD_{sq/hq}$ potential and increasing $\Delta E°$ at high pH, as observed for MMOR-FAD. In flavodoxin, neutralization of individual acidic residues via amide substitution does not eliminate the redox-linked pK_a observed for the flavin semiquinone/hydroquinone redox potential (*34*, *35*). Increasing numbers of acid-to-amide flavodoxin mutations, however, increase this potential in an additive manner, with average contributions of ~15 mV per substitution (*36*). Moreover, the pH dependence of the semiquinone/hydroquinone potential decreases progressively with the number of charge neutralizations (*34*). Thus, for flavodoxin, modulation of this redox potential appears to be controlled by the collective effect of multiple acidic residues surrounding the flavin cofactor (*34*, *35*). The pK_a values determined for MMOR-FAD may also be macroscopic quantities that reflect multiple protonation events with similar microscopic pK_a values.

The MMOR-FAD_{hq} pK_a of 6.0 is higher than that observed in many flavoproteins, most of which exhibit a pK_a of <5 for the hydroquinone oxidation state (*31*). Placement of a negative electrostatic field near the flavin cofactor could contribute to this phenomenon by destabilizing the anionic hydroquinone species (Scheme 1). In addition, removing a negative charge from this position in the flavodoxin E60Q mutant produces an optical change for the oxidized protein (*33*) very similar to that observed for FAD_{ox} at low pH, where the putative charge(s) would be neutralized by protonation. The pK_a of 7.1 observed for the FAD_{hq} optical spectrum might even correspond to the same carboxylate group(s); the presence of a negative charge on the flavin would be expected to increase the pK_a of nearby carboxylate groups, as suggested for flavodoxin (*32*).

By comparison of the preliminary MMOR-FAD NMR structure[2] and the structures of homologous proteins, including PDR (*19*), *Alcaligenes eutrophus* flavohemoglobin (*37*), and *Azotobacter vinelandii* NADPH:ferredoxin reductase (*38*), candidates for the negatively charged MMOR-FAD residue(s) were identified as Asp52, Glu85, and Asp90. In the other flavoproteins, these nonconserved residues are in or near homologous sequences having atoms ≤ 7 Å from the isoalloxazine N1, N3, or N5 position. Addition or removal of other charges near the flavin cofactor, or a conformational change that alters hydrogen bonding or solvent accessibility to the isoalloxazine ring system, may also contribute to the pH dependence observed for the MMOR-FAD optical spectra and redox potentials (*33*, *39*−*42*). More definitive assignment of the pK_a effects to specific protein residues awaits completion of the MMOR-FAD structure.

Interdomain Electron Transfer. Electron transfer from MMOR-FAD_{hq} to either Fd_{ox} or MMOR-FAD_{ox} occurs on a very slow time scale ($k = 1500$ M^{-1} s^{-1} at 25 °C and 100 M^{-1} s^{-1} at 4 °C, respectively). It is particularly interesting to compare the interdomain electron transfer rates for the separated domains with the corresponding step in MMOR reduction with NADH ($k = 90$ s^{-1} at 4 °C) (*16*). Presumably, the [2Fe-2S] and flavin cofactors in MMOR are positioned in an orientation amenable to electron transfer with minimal structural reorganization. The large effective rate decrease (at 25 °C) for the noncovalently linked domains suggests that cofactor proximity is extremely important for efficient electron transfer in MMOR.

In FNR (Figure 1), a flavoprotein electron transferase protein with a dissociable one-electron carrier, ferredoxin, transient noncovalent complexes between the flavin and [2Fe-2S] proteins afford relatively fast electron transfer [$k \approx 1500-7000$ s^{-1} (*19*)] between cofactors. The X-ray structure of a complex between maize leaf ferredoxin and FNR reveals an intermolecular interface comprising mainly electrostatic interactions in the form of salt bridges and a hydrophobic region between the cofactors (*43*). Precomplexing MMOR-Fd and MMOR-FAD before reduction with NADH did not significantly increase the observed interdomain electron transfer rates. This result implies that, unlike the ferredoxin−FNR system, the separated MMOR domains do not form a specific complex or that the complex that forms is unsuitable for efficient electron transfer. For full-length MMOR, in which the Fd and FAD domains are covalently tethered, high-affinity interdomain interactions are apparently unnecessary. Therefore, it appears that proximity rather than affinity facilitates interdomain electron transfer in MMOR.

Conclusions. This work demonstrates that the modular structure of MMOR can be exploited to simplify and extend characterization of a complex protein. Except for interdomain electron transfer, the separated MMOR-Fd and MMOR-FAD proteins retain biochemical properties essentially identical to those of the corresponding domains in MMOR. In simplifying a complicated system, these domains have already proved to be valuable for characterizing the structure and intramolecular electron transfer properties of the full-length reductase (*16*, *29*). Via examination of electron transfer to MMOH from both MMOR and MMOR-Fd, elucidation of the carefully orchestrated intermolecular electron transfer steps in the sMMO catalytic cycle will be possible.

ACKNOWLEDGMENT

We thank Dr. George T. Gassner for many helpful discussions and critical reading of the manuscript, Dr. Jens Müller for help with structural analysis, and Dr. Maarten Merkx for assistance in collecting EPR data. We also acknowledge the Multiuser Facility for the Study of Complex Macromolecular Systems (NSF-0070319) for access to an isothermal titration calorimeter.

REFERENCES

1. Higgins, I. J., Best, D. J., and Hammond, R. C. (1980) New findings in methane-utilizing bacteria highlight their importance in the biosphere and their commercial potential, *Nature 286*, 561−564.
2. Nguyen, H.-H. T., Elliott, S. J., Yip, J. H.-K., and Chan, S. I. (1998) The particulate methane monooxygenase from *Methylococcus capsulatus* (Bath) is a novel copper-containing three-subunit enzyme, *J. Biol. Chem. 273*, 7957−7966.
3. Prior, S. D., and Dalton, H. (1985) The effect of copper ions on membrane content and methane monooxygenase activity in methanol-grown cells of *Methylococcus capsulatus* (Bath), *J. Gen. Microbiol. 131*, 155−163.
4. Woodland, M. P., and Dalton, H. (1984) Purification and characterization of component A of the methane monooxygenase from *Methylococcus capsulatus* (Bath), *J. Biol. Chem. 259*, 53−59.

5. Green, J., and Dalton, H. (1985) Protein B of soluble methane monooxygenase from *Methylococcus capsulatus* (Bath), *J. Biol. Chem. 260*, 15795−15801.
6. Liu, K. E., and Lippard, S. J. (1995) Studies of the Soluble Methane Monooxygenase Protein System: Structure, Component Interactions, and Hydroxylation Mechanism, in *Advances in Inorganic Chemistry* (Sykes, A. G., Ed.) pp 263−289, Academic Press, San Diego.
7. Feig, A. L., and Lippard, S. J. (1994) Reactions of non-heme iron-(II) centers with dioxygen in biology and chemistry, *Chem. Rev. 94*, 759−805.
8. Wallar, B. J., and Lipscomb, J. D. (1996) Dioxygen activation by enzymes containing binuclear non-heme iron clusters, *Chem. Rev. 96*, 2625−2657.
9. Merkx, M., Kopp, D. A., Sazinsky, M. H., Blazyk, J. L., Müller, J., and Lippard, S. J. (2001) Dioxygen activation and methane hydroxylation by soluble methane monooxygenase: a tale of two irons and three proteins, *Angew. Chem., Int. Ed. 40*, 2782−2807.
10. Colby, J., and Dalton, H. (1978) Resolution of the methane monooxygenase of *Methylococcus capsulatus* (Bath) into three components, *Biochem. J. 171*, 461−468.
11. Gassner, G. T., and Lippard, S. J. (1999) Component interactions in the soluble methane monooxygenase system from *Methylococcus capsulatus* (Bath), *Biochemistry 38*, 12768−12785.
12. Merkx, M., and Lippard, S. J. (2002) Why OrfY? Characterization of MMOD, a long-overlooked component of the soluble methane monooxygenase from *Methylococcus capsulatus* (Bath), *J. Biol. Chem. 277*, 5858−5865.
13. Lund, J., and Dalton, H. (1985) Further characterization of the FAD and Fe_2S_2 redox centres of component C, the NADH:acceptor reductase of the soluble methane monooxygenase of *Methylococcus capsulatus* (Bath), *Eur. J. Biochem. 147*, 291−296.
14. Lund, J., Woodland, M. P., and Dalton, H. (1985) Electron-transfer reactions in the soluble methane monooxygenase of *Methylococcus capsulatus* (Bath), *Eur. J. Biochem. 147*, 297−305.
15. Stainthorpe, A. C., Lees, V., Salmond, G. P. C., Dalton, H., and Murrell, J. C. (1990) The methane monooxygenase gene cluster of *Methylococcus capsulatus* (Bath), *Gene 91*, 27−34.
16. Kopp, D. A., Gassner, G. T., Blazyk, J. L., and Lippard, S. J. (2001) Electron-transfer reactions of the reductase component of soluble methane monooxygenase from *Methylococcus capsulatus* (Bath), *Biochemistry 40*, 14932−14941.
17. Andrews, S. C., Shipley, D., Keen, J. N., Findlay, J. B. C., Harrison, P. M., and Guest, J. R. (1992) The haemoglobin-like protein (HMP) of *Escherichia coli* has ferrisiderophore reductase activity and its C-terminal domain shares homology with ferredoxin $NADP^+$ reductases, *FEBS Lett. 302*, 247−252.
18. Karplus, P. A., Daniels, M. J., and Herriott, J. R. (1991) Atomic structure of ferredoxin-$NADP^+$ reductase: prototype for a structurally novel flavoenzyme family, *Science 251*, 60−66.
19. Correll, C. C., Batie, C. J., Ballou, D. P., and Ludwig, M. L. (1992) Phthalate dioxygenase reductase: a modular structure for electron transfer from pyridine nucleotides to [2Fe-2S], *Science 258*, 1604−1610.
20. Gassner, G. T., and Ballou, D. P. (1995) Preparation and characterization of a truncated form of phthalate dioxygenase reductase that lacks an iron−sulfur domain, *Biochemistry 34*, 13460−13471.
21. Massey, V. (1957) Studies on succinic dehydrogenase. VII. Valency state of the iron in beef heart succinic dehydrogenase, *J. Biol. Chem. 229*, 763−770.
22. Stookey, L. L. (1970) Ferrozine: a new spectrophotometric reagent for iron, *Anal. Chem. 42*, 779−781.
23. Thompson, J. D., Higgins, D. G., and Gibson, T. J. (1994) CLUSTAL W: improving the sensitivity of progressive multiple sequence alignment through sequence weighting, position-specific gap penalties and weight matrix choice, *Nucleic Acids Res. 22*, 4673−4680.
24. Stainthorpe, A. C., Murrell, J. C., Salmond, G. P. C., Dalton, H., and Lees, V. (1989) Molecular analysis of methane monooxygenase from *Methylococcus capsulatus* (Bath), *Arch. Microbiol. 152*, 154−159.
25. Massey, V., and Hemmerich, P. (1980) Active-site probes of flavoproteins, *Biochem. Soc. Trans. 8*, 246−257.
26. Blazyk, J. L., Gassner, G. T., and Lippard, S. J., manuscript in preparation.
27. Walters, K. J., Gassner, G. T., Lippard, S. J., and Wagner, G. (1999) Structure of the soluble methane monooxygenase regulatory protein B, *Proc. Natl. Acad. Sci. U.S.A. 96*, 7877−7882.
28. Green, J., and Dalton, H. (1989) A stopped-flow kinetic study of soluble methane mono-oxygenase from *Methylococcus capsulatus* (Bath), *Biochem. J. 259*, 167−172.
29. Müller, J., Lugovskoy, A. A., Wagner, G., and Lippard, S. J. (2002) NMR structure of the [2Fe-2S] ferredoxin domain from soluble methane monooxygenase reductase and interaction with its hydroxylase, *Biochemistry 41*, 42−51.
30. Paulsen, K. E., Liu, Y., Fox, B. G., Lipscomb, J. D., Münck, E., and Stankovich, M. T. (1994) Oxidation−reduction potentials of the methane monooxygenase hydroxylase component from *Methylosinus trichosporium* OB3b, *Biochemistry 33*, 713−722.
31. Müller, F. (1992) Nuclear Magnetic Resonance Studies on Flavoproteins, in *Chemistry and Biochemistry of Flavoenzymes* (Müller, F., Ed.) pp 557−595, CRC Press, Boca Raton, FL.
32. Ludwig, M. L., Schopfer, L. M., Metzger, A. L., Pattridge, K. A., and Massey, V. (1990) Structure and oxidation−reduction behavior of 1-deaza-FMN flavodoxins: modulation of redox potentials in flavodoxins, *Biochemistry 29*, 10364−10375.
33. Geoghegan, S. M., Mayhew, S. G., Yalloway, G. N., and Butler, G. (2000) Cloning, sequencing and expression of the gene for flavodoxin from *Megasphaera elsdenii* and the effects of removing the protein negative charge that is closest to N(1) of the bound FMN, *Eur. J. Biochem. 267*, 4434−4444.
34. Swenson, R. P., and Zhou, Z. (1997) Role of Electrostatic Interactions in the Regulation of the One-Electron Reduction Potentials in the *Desulfovibrio* Flavodoxin, in *Flavins and Flavoproteins* (Stevenson, K. J., Massey, V., and Williams, C. H., Jr., Eds.) pp 427−436, University of Calgary Press, Calgary, AB.
35. Bradley, L. H., and Swenson, R. P. (1999) Role of glutamate-59 hydrogen bonded to N(3)H of the flavin mononucleotide cofactor in the modulation of the redox potentials of the *Clostridium beijerinckii* flavodoxin. Glutamate-59 is not responsible for the pH dependency but contributes to the stabilization of the flavin semiquinone, *Biochemistry 38*, 12377−12386.
36. Zhou, Z., and Swenson, R. P. (1995) Electrostatic effects of surface acidic amino acid residues on the oxidation−reduction potentials of the flavodoxin from *Desulfovibrio vulgaris* (Hildenborough), *Biochemistry 34*, 3183−3192.
37. Ermler, U., Siddiqui, R. A., Cramm, R., and Friedrich, B. (1995) Crystal structure of the flavohemoglobin from *Alcaligenes eutrophus* at 1.75 Å resolution, *EMBO J. 14*, 6067−6077.
38. Prasad, G. S., Kresge, N., Muhlberg, A. B., Shaw, A., Jung, Y. S., Burgess, B. K., and Stout, C. D. (1998) The crystal structure of NADPH:ferredoxin reductase from *Azotobacter vinelandii*, *Protein Sci. 7*, 2541−2549.
39. Bradley, L. H., and Swenson, R. P. (2001) Role of hydrogen bonding interactions to N(3)H of the flavin mononucleotide cofactor in the modulation of the redox potentials of the *Clostridium beijerinckii* flavodoxin, *Biochemistry 40*, 8686−8695.
40. Zhou, Z., and Swenson, R. P. (1996) The cumulative electrostatic effect of aromatic stacking interactions and the negative electrostatic environment of the flavin mononucleotide binding site is a major determinant of the reduction potential for the flavodoxin from *Desulfovibrio vulgaris* [Hildenborough], *Biochemistry 35*, 15980−15988.
41. Hoover, D. M., Drennan, C. L., Metzger, A. L., Osborne, C., Weber, C. H., Pattridge, K. A., and Ludwig, M. L. (1999) Comparisons of wild-type and mutant flavodoxins from *Anacystis nidulans*. Structural determinants of the redox potentials, *J. Mol. Biol. 294*, 725−743.
42. Ludwig, M. L., Pattridge, K. A., Metzger, A. L., Dixon, M. M., Eren, M., Feng, Y., and Swenson, R. P. (1997) Control of oxidation−reduction potentials in flavodoxin from *Clostridium beijerinckii*: the role of conformation changes, *Biochemistry 36*, 1259−1280.
43. Kurisu, G., Kusunoki, M., Katoh, E., Yamazaki, T., Teshima, K., Onda, Y., Kimata-Ariga, Y., and Hase, T. (2001) Structure of the electron transfer complex between ferredoxin and ferredoxin-$NADP^+$ reductase, *Nat. Struct. Biol. 8*, 117−121.

BI026757F